Ph.D. Dissertation of Science

Spatiotemporal variability of the horizontal salinity gradient and exchange flow over spring–neap tidal cycle in the Sumjin River estuary

섬진강 하구에서 대조–소조 조석 주기동안 수평염분구배와 교환류의 시공간 변동성

February 2023

School of Earth and Environmental Sciences

Graduate School

Seoul National University

Eun–Byeol Cho

Spatiotemporal variability of the horizontal salinity gradient and exchange flow over spring–neap tidal cycle in the Sumjin River estuary

Supervisor: Hanna Na, Professor

Submitting a Ph.D. Dissertation of Science
October 2022

School of Earth and Environmental Sciences
Graduate School
Seoul National University
Eun–Byeol Cho

Confirming the Ph.D. Dissertation written by
Eun–Byeol Cho
January 2023

Chair	Sung–Hyun Nam	(인)
Vice Chair	Hanna Na	(인)
Examiner	Duk–jin Kim	(인)
Examiner	Tae–Wan Kim	(인)
Examiner	Yong–Jin Tak	(인)

Abstract

Spatiotemporal variability of the horizontal salinity gradient and exchange flow over spring–neap tidal cycle in the Sumjin River estuary

Eun-Byeol Cho
School of Earth and Environmental Sciences
The Graduate School
Seoul National University

The distribution of salt, nutrients, pollutants, and suspended sediment in estuaries is mainly determined by the exchange flow. Although the exchange flow has been extensively studied, its variations during the spring–neap tidal cycle still need to be clarified. Many studies have indicated that the exchange flow is weaker during spring tides than during neap tides, but others have found that it is stronger during spring tides. Therefore, I investigated the spring-neap variation of an exchange flow and its cause based on intensive observational data and an analytical model applied to the Sumjin River estuary (SRE), Korea. The observations revealed that the horizontal salinity gradient was seven times larger and the exchange flow stronger during the spring tide than during the neap tide in the lower estuary. The analytical model demonstrated that the horizontal salinity gradient was a primary factor of exchange flow. During the

spring tide, the vertical shear of exchange flow was large due to the baroclinic forcing induced by the salinity gradient that was strong enough to overwhelm vertical mixing.

However, this result was limited to the lower estuary and could only represent part of the entire estuary. There have been few analyses of the horizontal salinity gradient and the fortnightly variation of exchange flow throughout the whole short estuary. I analyzed the variation in salinity gradient along the entire Sumjin River estuary and its effect on the exchange flow over fortnightly tidal cycles based on observations and numerical model experiments. The salinity gradient and exchange flow were in different phases between the lower and upper estuaries for 6-7 days. The maximum salinity gradient periodically reciprocated along the channel due to salt flux determined by vertical mixing. The stronger exchange flow (> 0.04 m s^{-1}) shifted from the mouth to the head of estuary while the tidal range decreased, resulting from variability of the horizontal salinity gradient. The horizontal salinity gradient was large enough to overwhelm the vertical mixing effect on the exchange flow in the entire estuary. This study suggests that it was crucial to determine the spatiotemporal variation in exchange flow throughout the estuary for the health of estuarine ecosystems.

The above results were conducted under the constant river discharge rate. However, most estuaries were subject to variable river flow conditions, which affected fortnightly variation in salinity distribution. The fortnightly variation of the horizontal salinity gradient and the factors determining the exchange flow were analyzed under various river discharge conditions. During low discharge conditions, the spring–neap variation of salinity gradient was not apparent. Still, as the discharge rate increased, the variation was pronounced, and the time of minimum salt intrusion gradually advanced to the spring tide. This was because as the time when the maximum salinity gradient appears in the lower estuary approaches the spring tide, the time when the salt flux was converted from seaward to landward accelerated due to the strengthening of exchange flow caused by baroclinic forcing. Depending on the river discharge rate, the exchange flow determinants differed. Vertical mixing was the main factor during low river discharge, but the salinity gradient was the main factor during over –mean discharge conditions. The spatial variation of exchange flow differed according to river discharge and tide. After all, to understand the circulation in the estuary, it was necessary to recognize that the spatial difference can vary depending on the forcing.

Keyword : exchange flow, horizontal salinity gradient, salt intrusion, fortnightly variation, Sumjin River estuary, ROMS

Student Number : 2013-20344

Table of Contents

List of Figures

List of Tables

1. General Introduction

1.1. Background

The estuary is "a semi-enclosed coastal body of water, which has a free connection with the open sea, and within which seawater is measurably diluted with fresh water derived from land drainage." (Pritchard, 1967). Estuaries are one of the most productive marine ecosystems on earth due to the high flux of nutrients from the land and serve as breeding and nursery grounds for many species (Ketchum, 1983; Neilson and Cronin, 1981). As many major cities are located next to estuaries, they also provide people with recreation, transportation, and water resources. Therefore, the impact of anthropogenic activity on the estuarine environment is a frequent concern (Kennish, 1986; Dyer, 1973). Assessing these impacts requires understanding the variability of circulation and stratification in the estuary.

The circulation and stratification in estuaries result from the interaction of the tides, river inflow, sea level fluctuations, winds, and bathymetry (Dyer, 1973). Their interaction changes the salinity gradient along the channel. The horizontal salinity gradient is a general characteristic of estuaries that shows a great diversity of

shape, depth, and forcing characteristics (Valle-Levinson, 2010). Typically, the salinity decreases from the ocean toward the head of the estuary due to freshwater input. The horizontal salinity gradient develops as the salinity becomes vertically homogenous by tidal mixing. The horizontal salinity gradient causes water masses to flat out their salinity layer (MacCready and Banas, 2011). In flattening, freshwater flows out near the surface, and ocean water enters near the bottom because more seawater must be drawn in to replace it. Therefore, the horizontal salinity gradient is one of the critical driving forces for the estuarine exchange flow, which plays a crucial role in maintaining salinity stratification in estuaries because the horizontal salinity gradient induces a vertically varying pressure gradient.

The estuarine exchange flow is subtidal (i.e., tidally averaged) along-channel velocity. It is an essential diagnostic for the flushing of an estuary, as it is responsible for transporting water parcels, nutrients, organisms, and pollutants through an estuary (MacCready and Banas, 2011) on timescales longer than a tidal cycle. The forcing characteristic that affects the exchange flow is very complicated due to the diversity of tidal currents, river discharge, turbulence, bathymetry, and salinity gradient. Among them, the main factors are salinity gradient and vertical mixing by the tide. The vertical shear

of the exchange flow is strengthened by the salinity gradient but weakened by vertical mixing.

In many estuaries, vertical movement of momentum and mass is active during the spring tide due to strong tidal mixing (Geyer and Cannon, 1982; Linden and Simpson, 1988; Monismith et al., 1996; Geyer et al., 2000; Stacey et al., 2010; MacCready and Geyer, 2010). The vertical difference in salinity is reduced, the velocity becomes vertically homogenous, and the horizontal salinity gradient develops. While the tidal range decreases and the vertical mixing weakens, the vertical difference in velocity and salinity increases due to the horizontal salinity gradient. Therefore, during the neap tide, the vertical shear of the exchange flow is large, and the stratification becomes strong. However, in some estuaries, the response of the stratification to the spring–neap variation was the same, but the response of the exchange flow responded differently (Park and Kuo, 1996; Becker et al., 2009). Park and Kuo (1996) presented a theoretical explanation that it could vary depending on the size of the estuary, and in particular, the opposite change could occur in small estuaries. Therefore, it is necessary to clarify how the exchange flow changes over the fortnightly tidal cycle and to analyze its mechanism in the short Sumjin River estuary.

1.2. Study area

The Sumjin River estuary is one of the few natural estuaries located in the center of the southern coast of Korea (Figure 1.1a, b). The Sumjin River discharges into Gwangyang Bay. According to the definition based on salinity distribution suggested by Pritchard (1967), an estuary would occupy the area at a river mouth where salinities range from approximately 0.1 to 30–35, the length of Sumjin River estuary is about 25km (Figure 1.1c). The scale of the estuary can be classified by a non–dimensional length parameter (δ), which is the ratio between the length of the estuary (L) and one–quarter of the tidal wavelength ($\lambda/4$), according to the definition of Li and O' Donnell (2005) as follows:

$$\delta = \frac{4L}{\lambda} \left(\lambda = \frac{\sqrt{gh}}{f} \right),$$

where g is the acceleration of gravity, h is the depth and f is the tidal frequency ($2.23 \times 10^{-5}\, s^{-1}$). An estuary with a δ value smaller (or larger) than 0.6-0.7 is defined as a short (or long) estuary. The Sumjin River estuary has a δ value of 0.27 and can therefore be classified as a short estuary. The estuary is relatively

narrow and shallow; the width and depth at the mouth are 1 km and 15 m, respectively, decreasing to 300 m and 2 m at the head. There are tributaries on the lower estuary side. However, based on data from Conductivity-Temperature-Depth (CTD) station 7, the east tributary has minimal effect on the salinity distribution of the main channel. A tributary on the west from station 4 flows mainly out of the estuary, with hardly any flow into the estuary.

The Sumjin River estuary is characterized by a semi-diurnal and fortnightly tidal cycle. The tidal form number was computed as the ratio of the main diurnal and semi-diurnal component amplitudes $(K_1 + O_1)/(M_2 + S_2)$ (Defant, 1960). It is measured at 0.22, indicating a semi-diurnal tide. The tidal range is about 3.4m during spring tide and 1.1m during neap tide. The M2 tide is the primary tidal constituent, and the amplitude of major five tidal constituents of M2, S2, N2, K1, and O1 are approximately 1 m, 0.47 m, 0.2 m, 0.19 m, and 0.12 m in amplitude, respectively. The estuary varies from partially mixed to well-mixed during spring tide and stratified during neap tide (Shaha and Cho, 2009). Tidal data were collected from the Gwangyang tidal gauge station operated by Korea Hydrographic and Oceanographic Agency (http://www.khoa.go.kr).

The climate of Korea is characterized by four seasons, and the discharge of Sumjin River is greatly affected by the monsoon rain and characterized by distinct changes between dry seasons (from November to April) and wet season (from July to October), with approximately 70% of total discharge in the wet season. The discharge data were obtained from the Songjung gauge station, operated by the Ministry of Construction and Transportation (http://www.wamis.go.kr) and located about 35km upstream from the estuary mouth. The average value is 20 m^3s^{-1} during the dry season and 180 m^3s^{-1} during the wet season based on the monthly mean discharge rate from 2001 to 2020. The monthly average for the entire period is 80 m^3s^{-1}.

Wind can be a dominant source of energy in large lakes, the open ocean, and some coastal areas, but it has a minor role in narrow small estuarine environments (Fischer et al., 1979) such as that in the SRE. The daily-mean wind speed observed by the Korea Meteorological Administration during the observation period was as weak as 0.7-1.5 m s^{-1} (Figure 1.1b AWS). Therefore, local or remote wind effects were not to be considered when analyzing the exchange flow. However, typhoons, which periodically pass over the study area, might alter the exchange flow in the SRE.

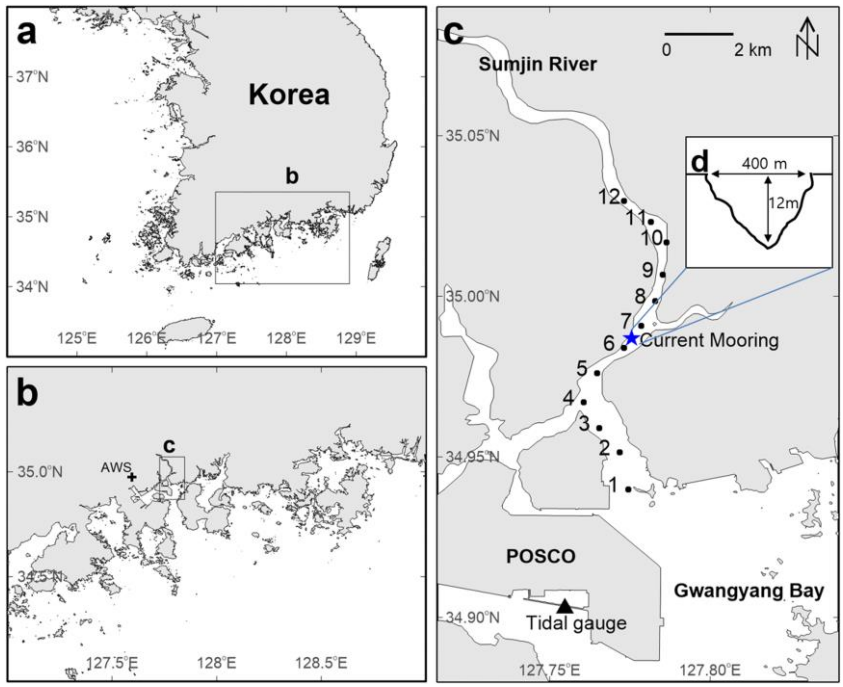

Figure 1.1 Study area: (a) Overview map of Korea; (b) Southern coastal area of Korea; (c) Sumjin River estuary study area, including the CTD stations 1–12 (black circles), current mooring station (blue star), and Gwangyang tidal gauge (black triangle).

1.3. Observations

An upward-looking Recording Doppler Current Profiler (RDCP, Aandera, 600kHz) was moored at about 6.5 km upstream from the mouth from October 19 to November 6, 2013, during two spring tides and one neap tide (Figure 1.1c). I used only the data for 20 days except for the start and end dates. The depth and width at the mooring point are approximately 12 m and 220m, respectively. The cell size is 2.0 m, and the cell overlap is 50%, which provides a 1 m vertical depth resolution. The blanking distance to the first cell is 1 m. The RDCP provides vertical velocity profiles with 1m depth bins from the surface to 3m above the bottom in a 10-minute time interval with a burst time of 132 s. The most upper and lower bins were discharged to avoid potential boundary interference affecting velocity measurements and thus to raise data reliability. Quality tests were done based on instrument tilting, the standard deviation of the records, and the signal/noise ratio of the beams.

To show the estuarine circulation along the channel more effectively, the north and east components of the current velocities were decomposed along the axis of maximum variance (45 ° west of north) to an along- and across-channel coordinate system, and the

along-channel velocity component (positive up-estuary) was considered in this study. I use u as the along-channel velocity component. All quality - controlled data were interpolated in terms of the non-dimensional depth (Z = z/H) from the surface (Z=0) down to the bottom (Z = -1.0) and averaged over a tidal cycle for the estuarine circulation.

The longitudinal hydrological data were acquired along the estuary from stations 1 to 12 on October 30, 2013 (Neap tide) and November 5, 2013 (Spring tide), using a YSI Castaway Conductivity-Temperature-Depth recorder operating at 5Hz. This instrument has an accuracy of 0.1 g kg^{-1} in salinity and 0.05 in temperature. The average spatial resolution between CTD stations was about 1 km. Observations were started at the first station 30 minutes before peak ebb and flood tide to obtain the vertical structure of salinity at the maximum flow rate. It usually took under 50 minutes to cast whole stations with experienced observation technology, so the observational data maintain the concurrence of the tidal phase.

These observational data could be used to analyze variations of the salinity distribution in the study area and to determine the horizontal salinity gradient. In order to investigate the characteristics

of the general salinity distribution, more observational data were analyzed. These data were observed twice a day during spring and neap tide in four seasons from 2004 to 2007. Eighteen times observations were used except for the period when the influence of the river tributaries was great.

Table 1.1 River discharge and tidal range during the CTD observations

Date	Discharge ($m^3 s^{-1}$)	Tidal range (cm)
April 30, 2004	46	277 (spring)
August 09, 2004	22	157 (neap)
October 16, 2004	29	359 (spring)
October 22, 2004	26	122 (neap)
January 29, 2005	14	310 (spring)
January 19, 2005	14	66 (neap)
April 08, 2005	18	353 (spring)
April 16, 2005	26	186 (neap)
August 10, 2006	51	315 (spring)
October 31, 2006	14	147 (neap)
April 03, 2007	19	306 (spring)
January 27, 2007	11	107 (neap)
October 30, 2013	22	392 (spring)
November 05, 2013	25	137 (neap)

2. Enhanced exchange flow during spring tide in the lower estuary[①]

2.1. Introduction

Exchange flow (also called estuarine circulation; Dijkstra et al., 2017) is the tidally averaged along-channel water flow driven by density, tidal rectification, river discharge, and tidally asymmetric mixing (Valle-Levinson, 2011) in estuaries. Exchange flow might play a significant role in the net exchange of material along the axis of the estuary because it is critical to the net (residual) circulation of estuarine systems.

Exchange flow in estuaries is mainly determined by the river discharge and horizontal salinity gradient (Stacey et al., 2010; Valle-Levinson, 2010; Geyer and MacCready, 2014). Buoyancy inputs from river discharge can enhance the exchange flow (Stacey et al., 2001; de Miranda et al., 2005; Geyer and MacCready, 2014). Wind and bathymetry also affect exchange flow. Horizontal depth variations induce residual circulation due to frictional and density differences

---

① The results of the presented work have been published in Cho et al. (2020).

between shoals and channels (Huzzey and Brubaker, 1988; Li and O'Donnell, 1997; Valle-Levinson and Schettini, 2016; Kim and Cho 2017). In addition, local wind along the channel could enhance or weaken estuarine exchange flow (Scully et al., 2005). The net flux in the entrance driven by remote wind may induce barotropic exchange in the estuary (Wang and Elliott, 1978; Wang et al., 1979; Garvine, 1985; Wong and Moses-Hall, 1998; Wong and Valle-Levinson, 2002).

In addition, tidal currents might cause variations in exchange flow according to tidal modulation (Jay and Smith, 1990; Simpson et al., 1990; Li and Zhong, 2009; Valle-Levinson, 2010). However, the response of exchange flow to tidal modulation remains unclear (Stacey et al., 2001; MacCready and Geyer, 2010). Many studies have investigated spring-neap tidal variations in exchange flow. Many have suggested that the exchange flow weakens during spring tides due to enhanced vertical mixing (Geyer et al., 2000; Bowen and Geyer, 2003; Weisberg and Zheng, 2003; MacCready and Geyer, 2010; Stacey et al., 2010). Furthermore, the increase in effective viscosity during the spring tide, due to a combination of an increase in tidal energy and a decrease in stratification, enhances vertical mixing and weakens exchange flow (Stacey et al., 2010).

By contrast, stronger exchange flows were observed at the bottom layer of the Cape Fear River estuary during higher tidal range conditions than during lower tidal range conditions. Increased vertical turbulent salt fluxes and bottom-generated mixing during the higher tidal range period result in the freshening of near-bottom water. The freshening of near-bottom water leads to the higher observed horizontal salinity gradient and the resulting increase in baroclinic acceleration, which increases the gravitational circulation in the lower water column during the higher tidal range period. (Becker et al. 2009). However, it is not easy to generalize the results from the Cape Fear River estuary study to all estuaries considering that it represents limited spatial and temporal observations. It has been proposed that the relative strength of the exchange flow between spring and neap tides can be reversed according to the ratio between the horizontal salinity gradient and vertical mixing. If the horizontal salinity gradient overwhelms the effect of vertical mixing, the exchange flow can become enhanced during spring tides.

In this study, I clarified the spring–neap variation of an exchange flow and revealed its main cause based on intensive observations in the Sumjin River estuary (SRE), which is a small and shallow estuary in Korea. Based on the results, I discussed the contributions of the

horizontal salinity gradient and vertical mixing to the exchange flow.

2.2. Results

2.2.1. Exchange flow during spring and neap tides

The maximum tidal current was 2-3 times larger during spring tides than during neap tides in the SRE (Figure 2.1). During spring tides, the maximum flood current was 49 cm s^{-1} in the middle layer (5 m from the bottom). The flow decreased in the surface and bottom layers due to the seaward river flow and bottom friction, respectively. The maximum ebb current was 64 cm s^{-1} near the surface. The ebb current decreased with depth due to bottom friction. During neap tides, the maximum flood current was 24 cm s^{-1} in the middle layer (4 m from the bottom). The maximum ebb current was 22 cm s^{-1} near the surface.

To more effectively examine the spring-neap variation in the exchange flow along the channel, the observed velocities were converted into a non-dimensional depth ($Z = z/H$) from the surface ($Z = 0$) to the bottom ($Z = -1.0$), where H and z are the total depth of the station and observed depth of the current, respectively (Figure 2.3a). The residual flow obtained by 36-h low-pass filtering appeared as a two-layer flow that flowed seaward in the upper layer

and flowed landward in the lower layer (Figure 2.3b). The vertical shear of the residual flow was larger during spring tide but smaller during neap tide.

The velocity profiles between the flood and ebb tides were asymmetric during the spring tides but relatively symmetric during the neap tide (Figure 2.3). The peak flood current speed is over 50 cm s^{-1} in the lower layer and about 20 cm s^{-1} in the surface layer, while the peak ebb current speed is about 60 cm s^{-1} in the surface layer and 30 cm s^{-1} in the lower layer during the spring tide. However, the vertical shear of the velocity is small during the neap tide. The average exchange flow over 36 h was stronger during the spring tides than during the neap tides.

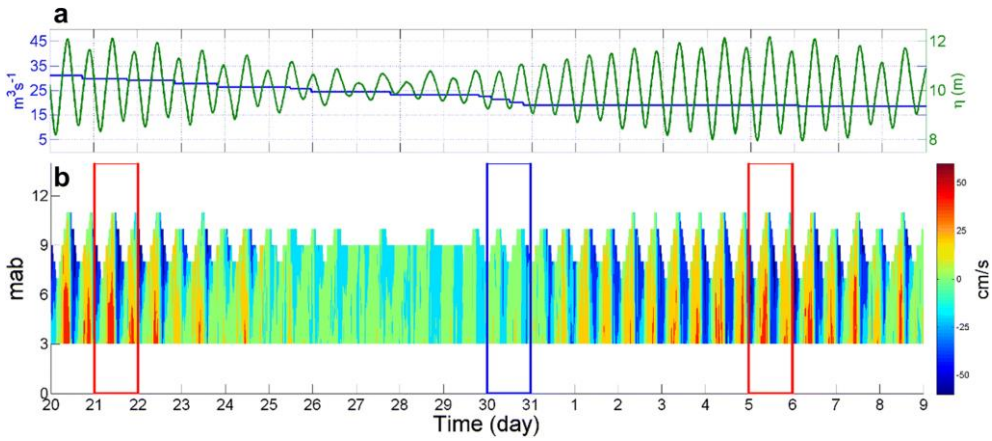

Figure 2.1 (a) Time series of river discharge (blue line) and surface elevation (green line) and (b) the along-channel velocity profiles. Positive signs indicate landward flow, and negative signs indicate seaward flow. Two spring tides (red boxes) and one neap tide (blue box) were selected for analyzing the variation in the exchange flow

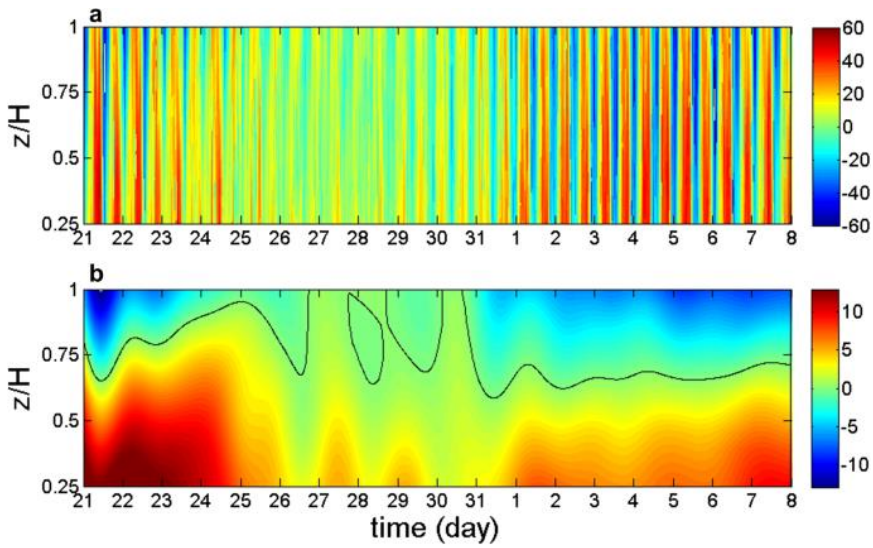

Figure 2.2 (a) Time series of the depth-normalized along-channel velocity profiles and (b) 36-h low-pass-filtered residual flow profiles. The black contour line indicates 0 m s^{-1}

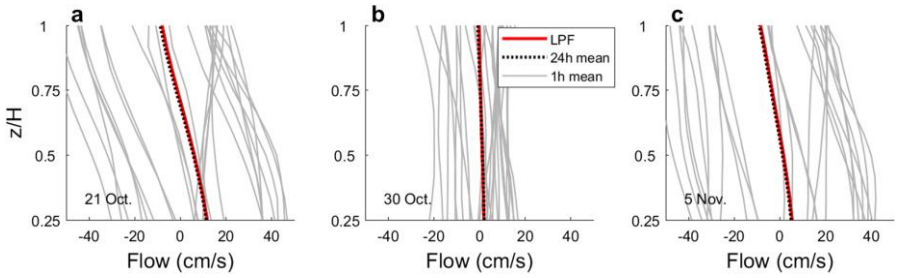

Figure 2.3 Hourly mean velocity profiles (gray lines–1−h mean), tidal mean velocity profiles (black dashed lines–24−h mean), and residual flows (25−h lowpass filtered) (red dotted lines–LPF) during two spring tides (a, c)and a neap tide (b) shown in the boxes in Figure 2.2b

2.2.2. Horizontal salinity gradients during spring and neap tides

The along-channel salinities observed during flood and ebb tides were averaged at each station to compare the salinity distribution between neap and spring tides. The salinity sections showed stratification during neap tides and destratification during spring tides (Figure 2.5). Following Hansen and Rattray (1966), the state of the estuary can be determined by $S_p = \delta s/\langle s \rangle$, where δs is the difference between the bottom and surface salinities, and $\langle s \rangle$ is the vertically averaged salinity. The estuary is stratified if $S_p > 0.32$ and is well mixed if $S_p < 0.15$ (Prandle, 1985). S_p was less than 0.15 during the spring tide, which indicated a well-mixed state. It was less than 0.3 (i.e., partially mixed) at the mouth but greater than 0.3 (i.e., stratified) during neap tide (Figure 2.6). Water with a salinity greater than 27 g kg^{-1} intruded along the bottom 11 km upstream of the estuary mouth during neap tides but only to 5 km during spring tide.

The depth-averaged salinities along the estuary were examined to calculate the horizontal salinity gradient during spring and neap tides (Figure 2.6). The salinities were the mean flood and ebb values during the spring and neap tides, respectively (Figure 2.6a). The

depth-averaged salinity during spring tides decreased landward as in typical coastal plain estuaries (Pritchard 1952; Hansen and Rattray 1965; Warner et al. 2005; Talke et al. 2009). However, the salinity exhibited a much smaller spatial variation during neap tides. The depth-averaged salinity decreased from 31 g kg^{-1} at the estuary mouth to 16 g kg^{-1} at 12 km upstream during spring tides and decreased from 29 g kg^{-1} to 23 g kg^{-1} during neap tides.

The horizontal salinity gradient was calculated from the depth-averaged salinities between neighboring stations at spring and neap, respectively (Figure 2.6b). The salinity gradients were similar at the mouth of the estuary but showed large differences in the middle estuary during spring and neap tides. The horizontal salinity gradient increased rapidly and reached a maximum of 2.5 g kg^{-1} km^{-1} at 10 km from the mouth during spring tides, whereas it decreased slowly until 9 km from the mouth during neap tides. The difference in the salinity gradient between the spring and neap tides reached a maximum at around 9 km from the mouth. Near the current mooring station (7 km from the mouth), the horizontal salinity gradient was about seven times greater during spring tides than during neap tides.

I analyzed the depth-averaged salinities and salinity gradients

using 24 observations with various river discharges and tidal ranges from 2004 to 2007 to compare with those in 2013. The salinities were the mean of the high and low water during spring and neap tides, respectively. The depth-averaged salinity decreased rapidly with distance from the estuary mouth during spring tides and decreased slowly during neap tides (Figure 2.6c).

The horizontal salinity gradient results were similar to those in 2013, except at the estuary mouth (Figure 2.6d). The salinity gradient at the estuary mouth was slightly smaller during spring tides but was about twice as large from 5 to 10 km during spring tides compared to neap tides. These observational results support the idea that the large horizontal salinity gradient during spring tides is a consistent structure in the middle estuary of the SRE, regardless of observation time.

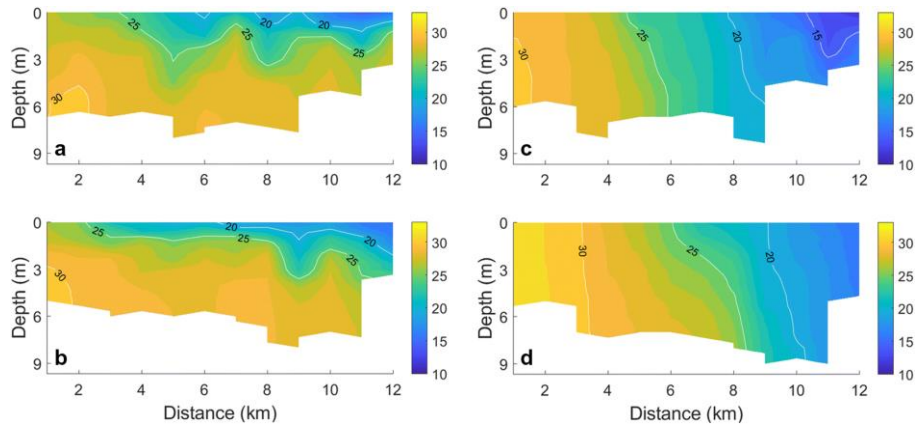

Figure 2.4 Vertical section of the salinity (g kg^{-1}) along the Sumjin River estuary from stations 1–12 during (a) flood and (b) ebb during the neap tide on October 30, 2013 and (c) flood and (d) ebb during the spring tide on November 5, 2013. The x-axis represents the distance from the mouth of the estuary

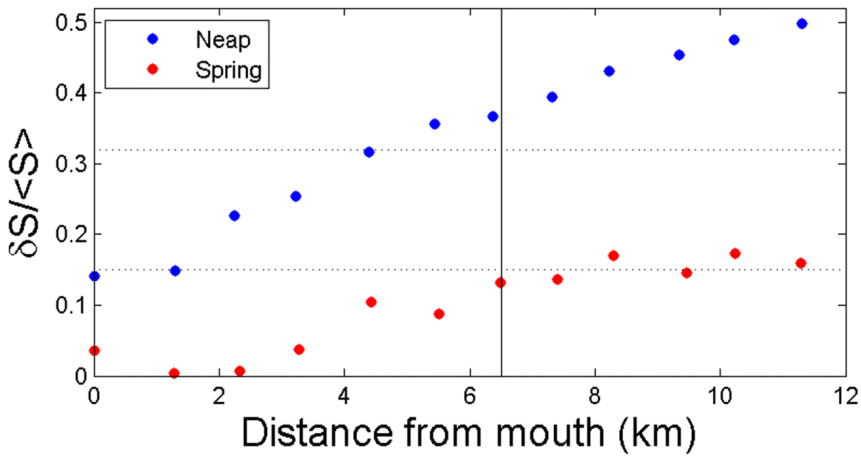

Figure 2.5 Stratification parameter for the Sumjin River estuary taken during both spring and neap tide. A value above 0.32 indicates a stratified condition and below 0.15 a well-mixed condition (dot lines). The vertical line indicates the mooring point

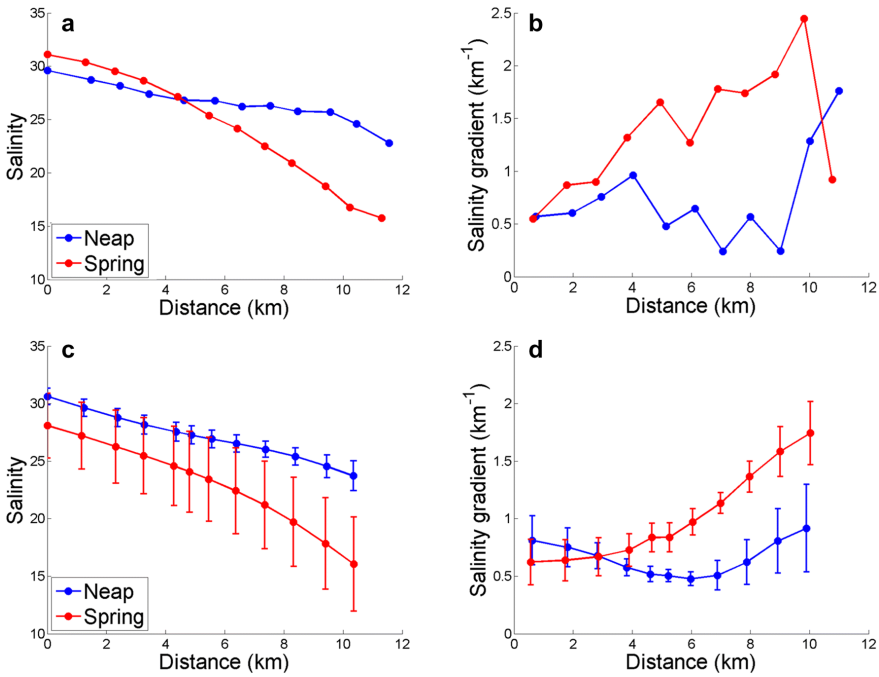

Figure 2.6 (a) Longitudinal distribution of the depth-averaged salinity during the spring tide (red circles and line) on November 5, 2013 and neap tide (blue circles and line) on October 30, 2013, (c) from 2004 to 2007. The filled circles indicate the location of the station. (b) Horizontal salinity gradient during the spring (red circles and line) and neap (blue circles and line) tides in 2013 and (d) from 2004–2007. The x-axis represents the distance from the mouth of the estuary.

2.2.3. Contribution of the horizontal salinity gradient to the exchange flow during spring and neap tides

The observational results revealed that the magnitude of exchange flow was more substantial, and the horizontal salinity gradient was higher during spring tides than during neap tides. The contribution of the horizontal salinity gradient to the exchange flow was estimated using an analytical model.

A number of studies have used a simple momentum balance equation containing surface slope, along-channel salinity gradient, and vertical mixing to clarify the main cause of the exchange flow (Hansen and Rattray, 1965; Officer, 1976; Talke et al., 2009; Pu et al., 2015). The governing momentum balance between the tidally averaged horizontal pressure gradient (barotropic and baroclinic pressure gradients) and vertical shear stress can be written as:

$$g\frac{\partial \eta}{\partial x} + \frac{g}{\rho_0}\frac{\partial \rho}{\partial x}H = A_z\frac{\partial^2 u}{\partial z^2}, \qquad (2.1)$$

where g is gravitational acceleration, η is the subtidal water surface elevation, x is the along-estuary direction (where positive values are landward), u is the along-estuary subtidal flow, z is the vertical direction (where positive values are upward), ρ_0 is the

reference density, and $\partial\rho/\partial x$ is the tidally averaged horizontal density gradient. A_z is the eddy viscosity (Valle-Levinson, 2010):

$$A_z = \frac{1}{48a_0} C_d U_a h, \tag{2.2}$$

where C_d is the bottom drag coefficient (0.0023), U_a is the amplitude of the depth-averaged tidal flow, which is 0.32 m s^{-1} during spring tide and 0.16 m s^{-1} during neap tide, and h is water depth (12 m). The calculated A_z was 0.0056 m^2 s^{-1} during spring tides and 0.0028 m^2 s^{-1} during neap tides. a_0, which is a dimensionless constant, was assumed to be 0.03 (Valle-Levinson, 2010). The boundary conditions with no stress at the surface ($\partial u/\partial z = 0\ at\ z = 0$) and zero velocity at the bottom ($u = 0\ at\ z = -H$) were assumed (Officer, 1976). The water slope could be expressed by applying the condition that the net transport per unit width was provided by the river discharge. Based on these conditions, the solution is:

$$\boldsymbol{u(z) = \frac{gH^3}{48\rho_0 A_z}\frac{\partial\rho}{\partial x}\left[9\left(1-\frac{Z^2}{H^2}\right)-8\left(1+\frac{Z^3}{H^3}\right)\right] + \frac{3}{2}\frac{R}{H}\left(1-\frac{Z^2}{H^2}\right) = U_D + U_R} \tag{2.3}$$

The left term $u(z)$ is the vertical profile of velocity resulting from the above balance. The first term (U_D) on the right side represents the flow driven by the horizontal density gradient, and the second term (U_R) describes the subtidal flow produced by the river discharge. ρ_0 was calculated to be 1018 kg m^{-3} during spring tides and 1017 kg m^{-3} during neap tides. The density in the estuary is mainly determined by the salinity in the estuaries. The horizontal salinity gradient ($\partial s/\partial x$) was 1.51 g kg^{-1} km^{-1} in the SRE during the spring tidesand 0.22 g kg^{-1} km^{-1} during the neap tide, and it was about seven times greater during the spring tide. The density gradient ($\partial \rho/\partial x$) was 1.23 kg m^{-3} km^{-1} during the spring tide and 0.2 kg m^{-3} km^{-1} during the neap tide. River discharge was 22 m^3 s^{-1} during the spring tide and 25 m^3 s^{-1} during the neap tide.

To quantify the performance of the model results, the skill parameter was used (Willmott, 1981; Warner et al., 2005; Zhong and Li, 2006; Vaz et al., 2007; Andutta et al., 2013; Toublanc et al., 2015):

$$\text{Skill} = 1 - \frac{\sum|U_T - U_O|^2}{\sum(|U_T - \overline{U_O}| + |U_O - \overline{U_O}|)^2}, \quad (2.4)$$

where U_O is the observed data, U_T is the corresponding value

calculated with the model in Eq. (2.3), and $\overline{U_O}$ is the depth-mean observation value. The skill parameter varies from 1 to 0, where 1 indicates a perfect fit, and 0 indicates complete disagreement between the observations and analytical model results. The model results validated with the skill parameter had calculated values of 0.96 for the neap tide and 0.99 for the spring tide, indicative of good agreement between the model results and observational data (Figure 2.8).

The analytical model results imply that the horizontal salinity gradient is the main driver of the spring-neap tide variation in exchange flow in the SRE. The increased horizontal salinity gradient during spring tides increases the strength of the baroclinic flow. The river-induced flow is weak due to the relatively small discharge. Therefore, the barotropic effect of river discharge on the exchange flow in the SRE is negligible during the observation period.

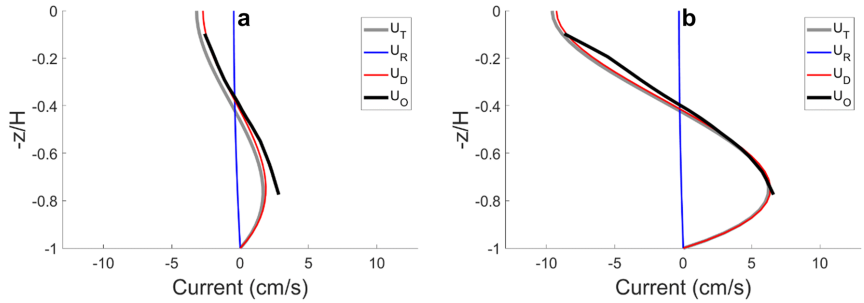

Figure 2.7 Comparison of the velocity profile at the current mooring station between analytical model results (U_T: gray lines) and observational data (U_O: thick black lines) during (a) the neap tide on October 30, 2013 and (b) the spring tide on November 5, 2013. U_R and U_D represent the calculated current driven by river discharge and density using the analytical model

Table 2.1 Variables for the tidal Froude number during spring tide (November 5, 2013) and neap tide (October 30, 2013).

Tide	U_a (m s^{-1})	H (m)	$\Delta\rho$ (kg m^{-3})	ρ (kg m^{-3})	$\boldsymbol{Fr_o}$
Spring	0.32	12	1.23	1016	0.71
Neap	0.16	12	0.20	1018	1.10

2.3. Discussion

The observations revealed that the exchange flow in the SRE increased because the horizontal salinity gradient is about six times greater during spring tide (1.51 g kg^{-1} km^{-1}) than during neap tide (0.22 g kg^{-1} km^{-1}). However, this contrasted with many studies in that tidally averaged flow was enhanced during the low tidal range (Geyer et al., 2000; Bowen and Geyer, 2003; Stacey et al., 2010).

Park and Kuo (1996) proposed that vertical mixing results in two opposing effects on exchange flow. One is the direct effect, that the exchange flow is weakened by enhancing the vertical momentum exchange when vertical mixing increases. The other is the indirect effect that strong vertical mixing decreases the salinities in the lower layer but increases those in the upper layer during spring tides (Becker et al., 2009). Stronger tidal forcing and associated mixing resulted in greater horizontal salinity gradients and increased baroclinic circulation (Park and Kuo, 1996; Becker et al., 2009). The relative contribution of both effects on the exchange flow can be estimated by γ, which is the fractional change in the horizontal salinity gradient and tidal current amplitude between the spring and neap tides:

$$\gamma = \frac{\left(\frac{\partial s}{\partial x}\right)_S}{\left(\frac{\partial s}{\partial x}\right)_N}\left[\frac{(U_a)_S}{(U_a)_N}\right]^{-1} = 3.43 \quad (2.5)$$

Here, the subscripts S and N are the variables during the spring and neap tides, respectively, $\frac{\partial s}{\partial x}$ is the horizontal salinity gradient. If γ is greater than unity, the exchange flow increases during spring tides because the horizontal salinity gradient overwhelms the vertical mixing effect. If γ is smaller than unity, the exchange flow decreases during the spring tides (Park and Kuo, 1996). The large γ (3.43) in the SRE suggests that the estuarine circulation is determined mainly by the horizontal salinity gradient.

γ can change within an estuary when the ratio of the horizontal salinity gradient between the spring and neap tides differs substantially. For example, the ratio of the salinity gradient at the mouth of the SRE between neap and spring tides decreased in 2013 and even reversed in past observations. This implies that the estuarine circulation at the mouth of the SRE may be weaker during spring tides than during neap tides, considering the stronger tidal current during spring tides.

γ can differ according to the size of the estuary. In this study, γ

was 3.43, based on our observations in the SRE with a length of 25 km. By contrast, the Rappahannock River estuary, which is over 70 km (~3 times longer than the SRE), γ was less than unity (Park and Kuo, 1996). Meanwhile, γ was 0.65 in the Modaomen estuary, with a length of 63 km (Gong et al., 2014), and 0.9 in the Cape Fear River estuary, with a length of 50 km (Becker et al., 2009). The response time of the salinity distribution can match the fortnightly tidal cycle, resulting in an increase in the horizontal salinity gradient in short estuaries during spring tide. However, the spring-neap cycle was short compared to the response time of the salinity distribution in long estuaries (Masson and Cummins, 2000). The timing of the maximum horizontal salinity gradient differs spatially in long estuaries.

The tidal Froude number, Fr_0, is a useful nondimensional number that compares the residual flows driven by density and by the tide (Valle-Levinson and Schettini 2016; Ross et al. 2017).

$$Fr_0 = \frac{{U_a}^2}{g'H}, \quad (2.7)$$

where U_a is the depth-mean tidal current amplitude, and g' is reduced gravity. The tidal Froude number at the mooring station in

the SRE was 0.71 during spring tide but 1.10 during neap tide (Table 2). This supports that the effect of the density gradient on the exchange flow in the SRE is more significant during the spring tide than during the neap tide.

2.4. Conclusion

Many studies have investigated exchange flows and their variations. However, the circulation's response to tidal modulation remains unclear. Therefore, I investigated the spring-neap tidal variation of an exchange flow with intensive observational data in the SRE, a narrow, short estuary in Korea. The observed currents showed that the vertical shear of exchange flow was strong during spring tides and weak during neap tides. The amplitude of the tidal current during spring tides was two times larger than that during neap tides.

Repeated CTD observations consistently showed that the horizontal salinity gradient was greater during spring tides than during neap tides. For example, the horizontal salinity gradient around the current observation station in the middle estuary was 1.51 g kg^{-1} km^{-1} during spring tides and 0.22 g kg^{-1} km^{-1} during neap tides. The analytical model results implied that the horizontal salinity gradient was the major cause of the exchange flow increase in the SRE during spring tides.

Our results are in contrast to many previous studies that found

that the exchange flow is weak during spring tides when vertical mixing is strong. Previous studies have reported that strong vertical mixing weakens the exchange flow because it enhances vertical momentum exchange.

Although the direct effects of the decrease in vertical mixing reduce the exchange flow, the indirect effects result in a large horizontal salinity gradient during spring tide. The ratio of the horizontal salinity gradient and vertical mixing between spring and neap tides (γ) provides their relative contributions to the exchange flow. The large γ of 3.43 suggests that exchange flow strength in the SRE is determined by the horizontal salinity gradient. The calculated Froude number support that the effect of the horizontal density gradient on the exchange flow in the SRE is more significant during the spring tide than during the neap tide. This is consistent with the observation that the exchange flow and horizontal salinity gradient are stronger during spring tides than during neap tides. The horizontal salinity gradient might depend not only on vertical mixing but on the size of the estuary. Future studies should examine the quantitative change in the horizontal salinity gradient according to the estuary and its dynamics.

3. Fortnightly variability of horizontal salinity gradient and exchange flow in the entire estuary[②]

3.1. Introduction

The transport and behavior of substances, such as pollutant sediments, organisms, and nutrients, largely depend on the strength of estuarine exchange flow. The exchange flow is the tidally averaged along-channel velocity through an estuarine cross-section (Geyer and MacCready, 2014; Stacey et al., 2001; Valle-Levinson, 2010) and is also referred to as estuarine circulation (Dijkstra et al., 2017; Geyer and MacCready, 2014). The vertical shear of the exchange flow is mainly determined by competition between vertical mixing and the horizontal salinity gradient (Garel and Ferreira, 2013; Mantovanelli et al., 2004; Park and Kuo, 1996; Stacey et al., 2001; Uncles and Stephens, 1990; Valle-Levinson, 2010). Increased vertical mixing enhances the vertical momentum flux, which weakens the vertical shear of exchange flow, whereas an increased salinity

② The results of the presented work have been published in Cho et al. (2022).

gradient strengthens the vertical shear. The intensity of vertical mixing and salinity gradient can vary depending on the tidal range, and the contention results of these two factors change fortnightly; this determines exchange flow (Park and Kuo, 1996).

Previous studies have proposed that fortnightly variation in the vertical shear of exchange flow is determined by turbulent mixing owing to the tide. During spring tides, vertical momentum exchange is active owing to strong vertical mixing, and exchange flow is weakened; during the neap tide, exchange flow is strong owing to decreased vertical mixing, as observed in many estuaries, such as the Hudson River estuary (Bowen and Geyer, 2003; Geyer et al., 2000; MacCready and Geyer, 2010; Scully et al., 2009), Modaomen estuary (Gong et al., 2014), Peruípe River estuary (Andutta et al., 2013), and Curimatau River estuary (de Miranda et al., 2005). On the other hand, recent studies of short estuaries (i.e., those that are shorter than the dominant tidal wavelength) have reported that the salinity gradient plays a major role in the exchange flow variation, which is stronger during the spring tide (Becker et al., 2009; Cho et al., 2020). In the Cape Fear River estuary, stronger tidal forcing and associated mixing contribute to increased estuarine circulation due to a greater near-bottom horizontal salinity gradient during the high

tidal range (Becker et al., 2009). In the Sumjin River estuary, the effect of the horizontal salinity gradient, which is six times higher during the spring tide compared with the neap tide, overwhelms the effect of vertical mixing, resulting in stronger exchange flow during the spring tide (Cho et al., 2020). However, as these studies were conducted only at specific points, the fortnightly variation of exchange flow over the whole short estuary remains unclear. In the study of the short Blackwater estuary, a semi-analytical approach was used. The analysis focused on lateral changes in residual circulation but did not examine spring-neap variation (Wei et al., 2022). Therefore, fortnightly variation of the vertical shear of exchange flow in the entire estuary is still poorly understood as the analysis has received little attention.

In this study, the variability of the horizontal salinity gradient and exchange flow during the fortnightly tidal cycle was analyzed for the entire short and narrow estuary based on observations and numerical model experiments. The estuary was simulated using a numerical model by simplifying the geometry of the Sumjin River estuary. The mechanism underlying periodic salinity gradient change and its effect on the exchange flow were investigated. A numerical experiment with realistic topography was conducted to examine its applicability to the

Sumjin River estuary.

3.2. Materials and Methods

3.2.1. Model description

I assumed a simplified Sumjin River estuary system that is well mixed or periodically stratified, forced with a steady river flow rate and two tidal constituents (M_2, S_2), resulting in fortnightly tidal variation. This particular configuration was designed to be as simple as possible in order to reproduce the spring-neap tidal variation observed in the Sumjin River estuary. The simulation was performed using the Regional Ocean Modeling System (ROMS), which solves the hydrostatic, incompressible, Reynolds-averaged momentum and tracer conservation equations with a terrain-following vertical coordinate and free surface (Shchepetkin and McWilliams, 2005).

The idealized model domain includes a bay between the open boundary and estuary mouth. To match the observations, I assumed that the estuary mouth was located 7 km from the boundary. The estuary was implemented in a straight line to exclude the effect of meandering. The cross-section was rectangular in shape, and the water depth and width followed a linear trend based on the actual change (Figure 3.1b, c). This simplification minimizes the nonlinear

effect caused by complex topography and focuses only on the fortnightly variation. However, since these settings are different from the friction effect in real geometry, the mixing parameterization should be elaborately tuned using a proper vertical mixing scheme and forcing. The vertical mixing was parameterized using the K-Profile Parameterization scheme (KPP; Large et al., 1994). In the Mellor-Yamada and GLS (k-kl, k-e, k-w) mixing schemes, the thickness of the thermocline was thinner than that of the KPP during the neap tide, and the length of inflow of the high salinity (> 28) water mass to the bottom layer was longer by 1-5 km. During the spring tide, all schemes similarly implemented strong vertical mixing, but in all schemes other than KPP, the inflow of the high salinity water mass was longer by 1-4 km. The vertically averaged salinity reduction rate along the channel and the inflow length of high salinity water were most similar to the observation in the KPP.

The idealized model was constructed with 110 (along-channel, y-direction) × 17 (cross-channel, x-direction) grids and ten (vertical, z-direction) vertical layers. The along-channel grid size (Δy) was 340 m, the cross-channel grid size (Δx) was 34-190 m, and the 10 vertical layers were uniformly discretized. The model was forced by river flow at the northern end of the estuarine channel, and

two tidal components were imposed at the southern boundary. The inflowing river discharge rate was 60 m^3 s^{-1} , with a salinity of 0 g kg^{-1} , which was suitable for an idealized model. The salinity at the ocean boundary was 35 g kg^{-1} , and the initial salinity was set to 20 g kg^{-1} . The temperatures at the open boundary and river inflow were set to 20 ° C, the same as the background temperature set throughout the entire domain. The open boundary was treated with the Champman condition for surface elevation, Flather condition for barotropic velocity, and Clamped boundary conditions for open-ocean salinity. The other forcing was a tidal sea surface height variation on the open boundaries at the M_2 and S_2 frequencies. The idealized model was integrated for 100 days with a baroclinic time step of 10 s. The idealized model presented a steady spring-neap tidal cycle in the salinity field after a spin-up period of 30 days, after which it was run for another 70 days to capture several fortnightly tidal cycles.

The realistic model (Figure 3.1d) was constructed with 158 (along-channel, y-direction) × 14 (cross-channel, x-direction) grids and 10 (vertical, z-direction) vertical layers. The along-channel grid size (Δy) was 10-540 m, the cross-channel grid size (Δx) was 6-240 m, and the ten vertical layers were uniformly

discretized. Like the idealized model, the realistic model was forced by river flow and the two tidal components at the northern and southern boundaries. The initial and boundary values of salinity and water temperature were also the same as in the idealized model. The realistic model was integrated for 100 days with a baroclinic time step of 2 s. The realistic model presented a steady spring-neap tidal cycle in the salinity field after a spin-up period of 30 days, after it had been run for another 70 days to capture several fortnightly tidal cycles.

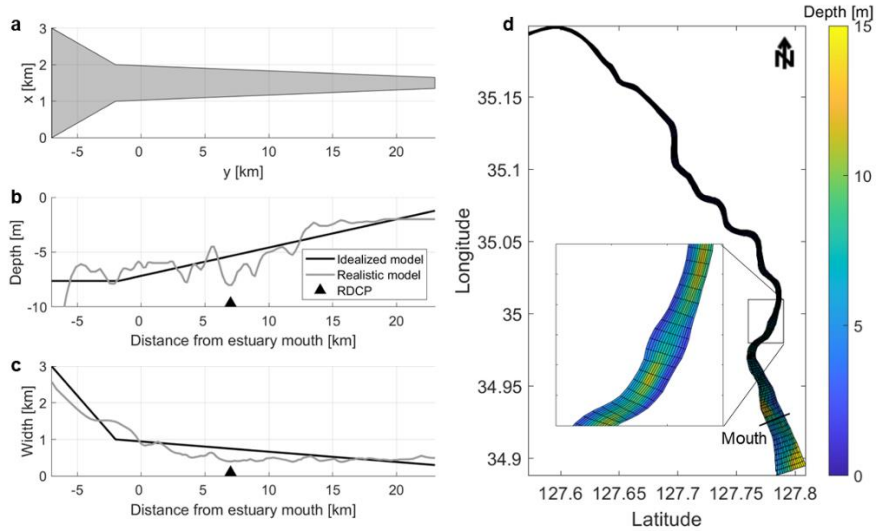

Figure 3.1 Idealized model domain information. (**a**) Idealized estuary model domain and the along−channel variations of (**b**) depth and (**c**) width for the model (black lines) and observations (grey lines) in the Sumjin River estuary. The observation depth is laterally averaged. The black triangles indicate the velocity observation station in Figure 3.1b RDCP. (**d**) Realistic model domain with depth (m); the estuary mouth is indicated by the black line.

3.2.2. Comparison of salinity and current between observations and models

The model was designed to simulate the fortnightly variability of salt distribution in the Sumjin River estuary, and the model results were compared with the observations. The current velocity was observed at one point, and salinity at 12 stations along the channel up to 12 km upstream from the mouth. The salinity in the model was in good agreement with that observed at most stations (Figure 3.3). The root-mean-square error for all the stations in the idealized (realistic) model was 0.68 (3.4) and 0.48 (1.68) g kg^{-1} for depth-averaged salinity along the channel and 0.51 (0.46) and 0.35 (0.48) g kg^{-1} km^{-1} for the horizontal salinity gradient during the spring and neap tides, respectively. Model salinity sections were vertically mixed as observed during the spring tide, while stratified more strongly than observed during the neap tide. However, both models reproduced well that the salinity gradient was up to 7 times larger during the spring than during the neap tide, which was a significant feature in observation.

The horizontal salinity gradient may vary depending on the horizontal length scale (Geyer et al., 2000) and the depth to be used.

Therefore, I needed to check whether there was a change in the fortnightly variation of the salinity gradient. So, when calculating the salinity gradient with the observed salinity, the horizontal length was changed to 1-10 km intervals. When the salinity was averaged vertically, the water depth from the surface layer was also applied differently. As the horizontal interval increased, the horizontal salinity difference also increased, and the salinity gradient decreased only slightly. There was almost no difference even when the salinity gradient was calculated by averaging the salinity based on various water depths. In the analytical model using the balance equation of pressure gradient and friction (Cho et al., 2020), the observed exchange flow was well realized when the horizontal length scale was set at a 1 km interval when calculating the salinity gradient. Therefore, I used the salinity from the surface layer to the bottom and set the horizontal length to 1 km to calculate the salinity gradient.

A comparison of the depth-averaged along-channel velocity between the model and the observations indicated that the phase was properly simulated; however, the magnitude was overpredicted in the model (Figure 3.4a). When the tidal range was small, the difference in magnitude was approximately 15 $\mathrm{cm\,s^{-1}}$, which decreased to 7 $\mathrm{cm\,s^{-1}}$ at a large tidal range. The exchange flow in observations and

the model was compared (Figure 3.4b). The exchange flow was calculated using a 25-hour low pass filter (MATLAB R2021b function: all subsequent low pass filters used this tool) for the observation results at a 10 min interval and for the model at a 1-hour interval to suppress semi-diurnal tidal variability. I tried different timeframes (25 - 72 h) for the low pass filter, and the results were all similar. The vertical shear of the exchange flow observed at the lower estuary was greater during spring tides than during neap tides. The model captured the difference in the vertical velocity profile between the two periods well.

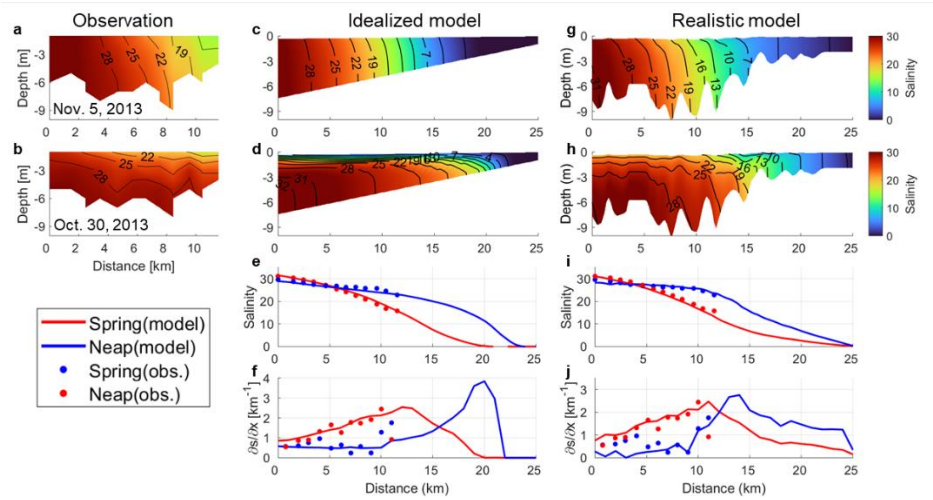

Figure 3.2 Comparisons of salinity among observations, an idealized model, and a realistic model. Vertical sections of the along-channel salinity during (a, c, g) the spring tide and (b, d, h) neap tide in (a, b) observations, (c, d) the idealized model and (g, h), and the realistic model. Variations in depth-averaged (e, i) salinity and (f, j) horizontal salinity gradient from mouth to head during spring (red) and neap tides (blue). Dots and lines denote observations and model outputs, respectively.

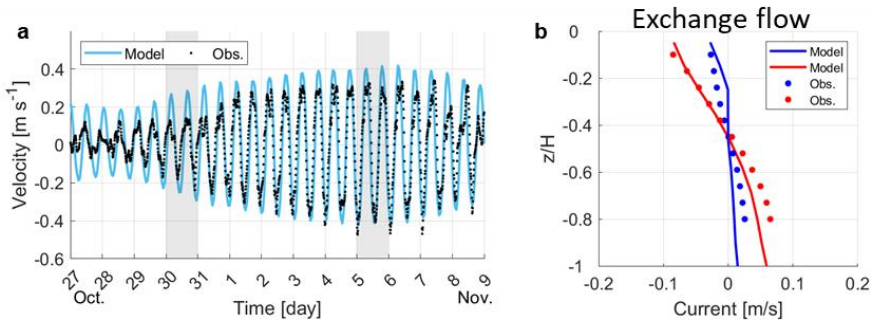

Figure 3.3 Comparison of flow rates between observations and the idealized model. (**a**) Time series of the depth−averaged velocity in observations (black dots) and the model (cyan line), with grey shading indicating Conductivity–Temperature–Depth (CTD) observation dates. (**b**) Vertical velocity profile of the observations (dots) and model (lines) during spring (red) and neap (blue) tides denoted by CTD observation data (grey shading boxes) in (**a**).

3.2.3. Decomposition of salt flux

The salinity distribution and the horizontal salinity gradient were estimated based on the salt flux. The along-channel salt flux was divided into seaward and landward fluxes (Fischer, 1972; Hunkins, 1981; MacCready, 2007). The driving mechanisms of the salt flux were examined by applying the flux decomposition method proposed by Lerczak (2006).

The area-integrated, total along-channel salt flux was calculated as follows:

$$\boldsymbol{F} = \langle \iint \boldsymbol{vsdA} \rangle, \tag{3.2}$$

where the angled bracket denotes the tidal average; $\boldsymbol{dA}$ denotes the cross-sectional area of the individual grid cells estimated by multiplying $\boldsymbol{dx}$ and $\boldsymbol{dz}$, where $\boldsymbol{dx}$ and $\boldsymbol{dz}$ are determined by the horizontal and vertical sizes of the individual grid cells in the cross-sectional areas. Note that $\boldsymbol{dz}$ is time-dependent owing to the changes in surface height, while $\boldsymbol{v}$ and $\boldsymbol{s}$ are the temporal along-channel velocity and salinity, respectively.

The cross-sectional area $\boldsymbol{A}$ at a particular along-channel location is divided into a constant number of differential elements $\boldsymbol{dA}$

that constrict and expand with the tidal rise and fall of the free surface, respectively. The tidally averaged area (A_0) property is defined as follows:

$$\boldsymbol{dA_0 = \langle dA \rangle, A_0 = \langle \iint dA \rangle,} \tag{3.3}$$

where $\iint$ indicates the cross-sectional integral. Assessment of the contribution of the different processes to the salt fluxes requires decomposing the along-channel velocity and salinity fields into three components, which is the same as Lerczak (2006): both tidally averaged over a tidal period and the area of cross-section component (v_0, s_0), tidally averaged and cross-sectionally varying component (v_E, s_E), and tidally and cross-sectionally varying component (v_T, s_T):

$$v_0 = \frac{\langle \iint v dA \rangle}{A_0} \tag{3.4}$$

$$v_E = \frac{\langle v dA \rangle}{dA_0} - v_0 \tag{3.5}$$

$$v_T = v - v_E - v_{0,} \tag{3.6}$$

There is a corresponding set of equations for the salinity. The variable v_0 is related to the river flow volume flux $Q_0[= -v_0 A_0]$, v_E is the estuarine exchange flow, and v_T represents tidal current. The tidal varying components v_T and s_T satisfy $< v_T dA >= 0$ and $< s_T dA >= 0$. Then, the total along-channel salt flux can be calculated

as:

$$\boldsymbol{F} = \left\langle \iint (\boldsymbol{v_0} + \boldsymbol{v_E} + \boldsymbol{v_T})(\boldsymbol{s_0} + \boldsymbol{s_E} + \boldsymbol{s_T})\boldsymbol{dA} \right\rangle$$

$$= \iint (v_0 + v_E)(s_0 + s_E)dA_0 + \iint < v_T s_T dA > + cross\ terms$$

$$= \underbrace{-Q_0 S_0}_{F_R} + \underbrace{\iint v_E s_E dA_0}_{F_E} + \underbrace{\iint < v_T s_T dA >}_{F_T} \qquad (3.7)$$

Where the cross terms have been dropped because the results are negligibly small uncorrelated by denifiton. Under this decomposition, F_R is the advective salt flux due to the river outflow, which is always a seaward salt flux; F_E is the salt flux resulting from steady shear dispersion, which is the spatial correlation of tidally averaged velocity and salinity; and F_T is the cross-sectionally integrated tidal oscillatory salt flux due to the correlation among tidal variations in velocity, salinity, and depth. In this paper, I use the low pass filter with 25 h to obtain the tidally averaged values.

3.3. Results and Discussion

I primarily analyzed the results of the idealized model to exclude nonlinear effects caused by complex topography and focus on spring–neap variations. The realistic model results in 3.3.4 were referred to confirm that main findings are applicable to the actual estuary.

3.3.1. Periodic propagation of the horizontal salinity gradient

First, the spatiotemporal variability of the salinity distribution, which determines the horizontal salinity gradient, was investigated. In order to focus on the fortnightly variation of the salinity distribution, salinity at a 1–hour interval from the model was low pass filtered (25–hour) and sectionally averaged (Figure 3.4). The salinity distribution varied periodically (Figure 3.4b). During spring tides, the salt intrusion length was the shortest, the vertical salinity difference was less than 2, and it was vertically well–mixed (Figure 3.4c), so the horizontal difference of salinity was large. During neap tides, the salt intrusion length was the longest, and stratification was

strong, and so the horizontal difference in salinity was small.

The variability of salt transport determines the variation in the length of the salt intrusion. Based on the commonly used subtidal salt flux decomposition for estuaries, the seaward salt flux due to river outflow was balanced by the landward salt flux due to the upstream dispersive mechanism (Garcia et al., 2022; Lerczak et al., 2006; MacCready, 2007; Ralston and Stacey, 2005). The composition of each salt flux was estimated using the decomposition method (Chen et al., 2012; Lerczak et al., 2006; MacCready, 2011). The total horizontal salt flux (F) exhibited marked fortnightly variability (Figure 3.5a). The fluctuation in F implied that the estuary gains salt when the tidal range decreases but loses salt when the tidal range increases. As the landward of the salt flux continued, the salt intrusion became longer, and as the seaward salt flux continued, the salt intrusion became shorter. Salt was imported by F_E and F_T, and F_E contributed approximately 80% of the total landward salt flux, on average, during the fortnightly tidal cycle (Figure 3.5b). The diffusive fraction of landward salt flux ($\nu = F_T/(F_T + F_E)$) after Hansen and Rattray (1966) was generally less than 0.5 when the total salt flux was landward. It also proved that the steady shear dispersion salt flux (F_E) was dominant in the landward salt flux.

The horizontal salinity gradient along the channel also exhibited distinct fortnightly variation (Figure 3.6a). During spring tides, the salinity gradient was relatively high from the mouth and was the highest (> 2.0 g kg^{-1} km^{-1}) around the middle estuary (~10 km from the mouth). While the tidal range was decreasing, the maximum salinity gradient propagated to the head of estuary, becoming larger and reaching at least 5.0 g kg^{-1} km^{-1} during neap tides. Then, while the tidal range increased, the maximum salinity gradient retreated from the head. Thus, the fortnightly variation of the maximum salinity gradient was out of phase between the lower and upper estuary (Figure 3.6b). The time-varying maximum salinity gradient was similar to the results from the Hudson River estuary (Geyer and Ralston, 2015; Ralston et al., 2008). However, the maximum salinity gradient was maintained at the head without changing the position until the following spring tide in the Hudson River estuary, which differs from the Sumjin River estuary. Owing to its long length, the salinity distribution in the Hudson River estuary could not immediately respond to the tidal cycle in the upper estuary (Park and Kuo, 1996; Lerczak et al., 2009). Therefore, the maximum salinity gradient in the upper estuary may persist.

In the estuary of this study, the continuous movement of a high

salinity gradient along the channel was related to the convergence of the salt flux, $(\partial F/\partial x)$ The stronger the convergence became, the greater the horizontal difference in salinity, and a salinity gradient occurred. As the convergence decreased, the horizontal difference in salinity decreased. That was, the convergence of the salt flux could determine the movement of the maximum salinity gradient zone. Figure 3.6c showed the spatiotemporal change of the convergence of the salt flux. When the total salt flux was landward (seaward), the greater the positive (negative) value, the stronger the convergence. While the tidal range decreased after a spring tide, salt was imported into the estuary owing to the steady shear dispersion salt flux. As the salt intrusion length became longer, the high salinity gradient propagated toward the head of the estuary. The convergence of the salt flux also became more robust as it moved toward the estuary head, especially from 12 km to the head. As a result, the salinity gradient increased from 2 to 6 g kg^{-1} km^{-1} from the middle estuary to the head. While the tidal range increased after the neap tide, salt was exported out of the estuary owing to the advective salt flux. As the salt intrusion length was shortened, the salinity gradient also moved toward the mouth. A salinity gradient of 2 g kg^{-1} km^{-1} or more moved toward the mouth due to constant convergence in the seaward

direction. As such, the salinity gradients in the lower and upper estuary had different time changes (Figure 3.6b), which had a significant effect on the exchange flow.

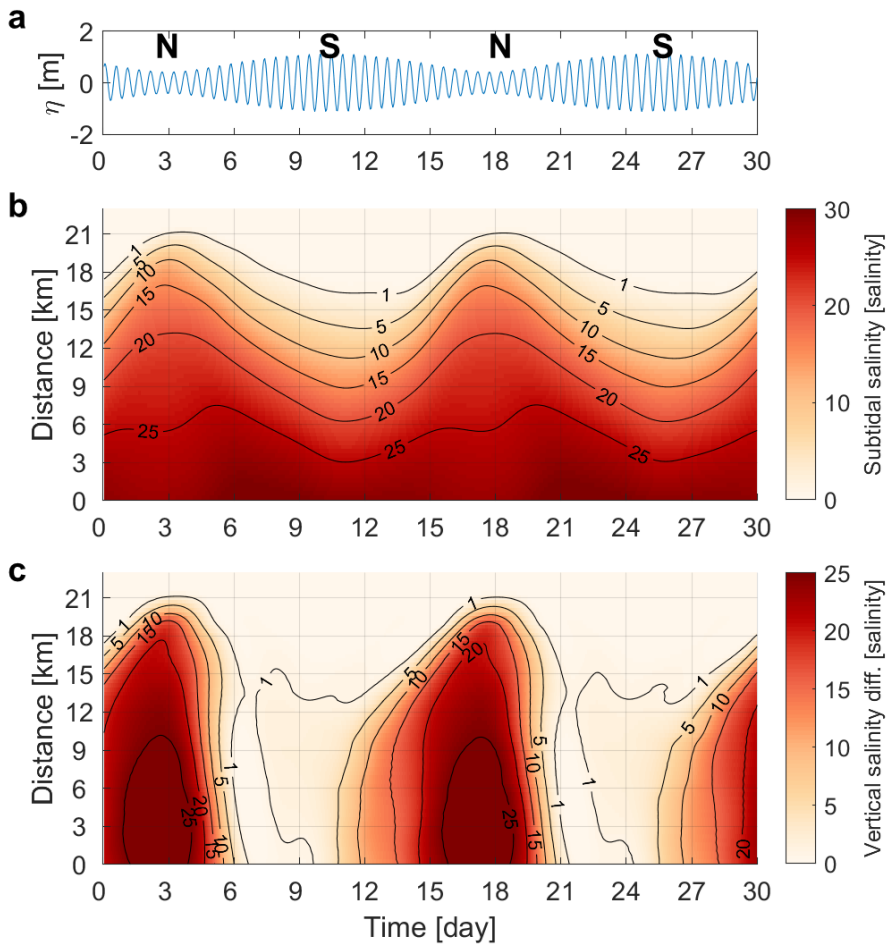

Figure 3.4 (a) Time series of sea-level height at the mouth of the idealized estuary and the N and S stand for neap tide and spring tide, respectively. Hovmöller diagram of (b) sectionally averaged subtidal salinity (unit: g kg^{-1}) and (c) the difference in salinity between the surface and bottom layer.

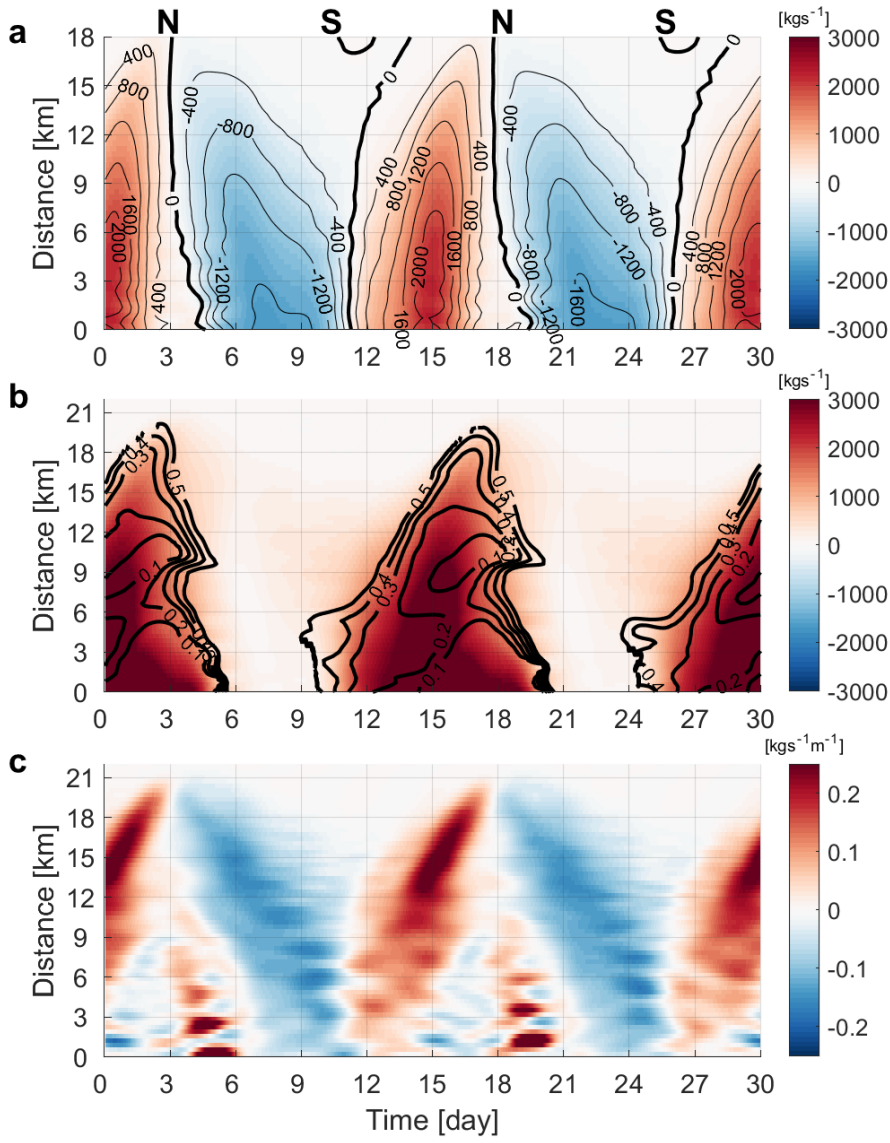

Figure 3.5 Hovmöller diagrams of the (a) total horizontal salt flux (F), (b) landward salt flux (color shading: steady shear dispersion salt flux [F_E] tidal oscillatory salt flux [F_T] unit: kg s^{-1}) and diffusive fraction (ν; black contour lines), and (c) convergence of total salt flux (unit: kg s^{-1} m^{-1}).

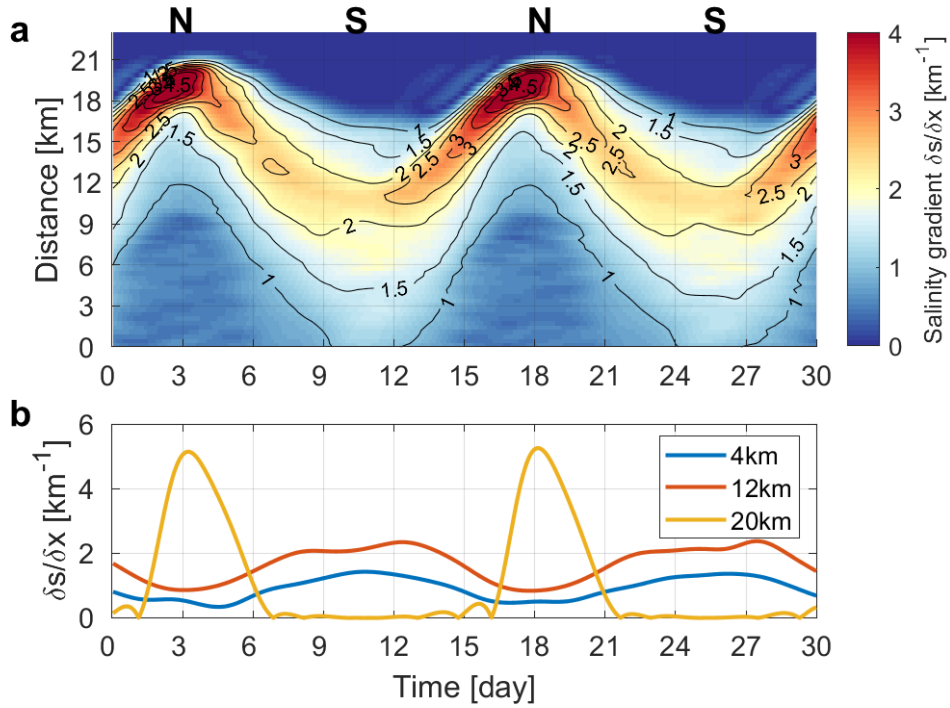

Figure 3.6 Hovmöller diagram of (a) horizontal salinity gradient along the channel (unit: g kg^{-1} km^{-1}) and (b) time series of salinity gradient at 4, 12, and 20 km.

3.3.2. Fortnightly variation in exchange flow and its cause

To analyze the fortnightly variation of exchange flow in the entire estuary, I calculated the intensity of exchange flow by averaging the absolute values with depth (Burchard et al., 2011). If the intensity is 0.04 or more (unit: $\mathrm{m\,s^{-1}}$), the exchange flow can be set as strong because at this intensity, F_E due to the exchange flow can induce the total salt flux landward. Uniquely, the exchange flow was strong (> 0.04 $\mathrm{m\,s^{-1}}$) in the lower and middle estuary around the spring tide and was generally weak during the increasing tidal range but strong during decreasing tidal range (Figure 3.7a). Therefore, there was a phase difference depending on the location (Figure 3.7b). In the lower estuary, it was at a maximum around the spring tide and a minimum after 2-3 days of the peak neap tide. In the upper estuary, it was strongest before and after the neap tide and weakest during the spring tide.

In a previous study of the Sumjin River estuary, the salinity gradient was the main determinant in the fortnightly variation of exchange flow in the lower estuary (Cho et al., 2020). To determine what mechanism caused the variation in the intensity of the exchange

flow in the entire estuary, I compared the salinity gradient and vertical mixing effect, which were the main factors determining the vertical shear of the exchange flow. The horizontal Richardson number (Ri_x), also referred as the Simpson number, has been used to provide a diagnostic balance between baroclinic forcing and vertical mixing due to tidal friction (Li et al., 2018; Stanev et al., 2015). I calculated Ri_x according to previous studies (MacCready and Geyer, 2010; Rayson et al., 2017) to identify the main factor that determines the exchange flow:

$$Ri_x = \frac{g\beta H^2(\partial s/\partial x)}{C_d {u_b}^2}, \tag{3.8}$$

where β is the saline contraction coefficient (7.7×10^{-4}) (Wang et al. 2015), g is the acceleration due to gravity, $\partial s/\partial x$ is the horizontal salinity gradient, H is the local water depth, C_d (4.0×10^{-3}) is the drag coefficient (used in the model setting), and u_b is the amplitude of the bottom tidal velocity (Stacey et al., 2001). There was considerable variation in the estimate of the critical value for Ri_x (MacCready and Geyer, 2010); it was less than 1 or set to 3 (Li et al., 2018; MacCready and Geyer, 2010; Stacey et al., 2001). Since I used the bottom tidal velocity, vertical mixing was weaker than when

using the depth−mean tidal velocity (Li et al., 2018; Pein et al., 2014; Schulz et al., 2015; Stanev et al., 2015) and the salinity gradient was large; therefore, the Ri_x was generally higher than 1. As such, I set the critical value to 3 in order to identify the main factor that strengthens the vertical shear of the exchange flow.

The baroclinic forcing and vertical mixing, which were determined Ri_x, differed in the timing and location of their strong appearance (Figure 3.8a, b). Baroclinic forcing had out−of−phase variability between lower and upper estuaries, but vertical mixing exhibited relatively in−phase variability. According to Eq. (3.8), baroclinic forcing was mainly determined by the horizontal salinity gradient. Therefore, the subtidal variation in baroclinic forcing was nearly consistent with the horizontal salinity gradient. During tidal range decreases, the exchange flow became stronger toward the head of the estuary because vertical mixing gradually decreased. However, the baroclinic forcing effect became predominant as the maximum salinity gradient moved to the head ($Ri_x > 3$). After the neap tide, as the tidal range increased, vertical mixing became stronger throughout the estuary, the baroclinic forcing effect became insignificant ($Ri_x \approx 1$), and the vertical shear of exchange flow weakened. The spatiotemporal changes with high Ri_x (> 3) and

strong exchange flow (> 0.04 m s^{-1}) agreed relatively well. Therefore, the salinity gradient determined the fortnightly variation of exchange flow not only in the lower estuary but also in the entire estuary. The phase difference occurred in the lower and upper estuaries because the salinity gradient was out of phase between lower and upper estuaries.

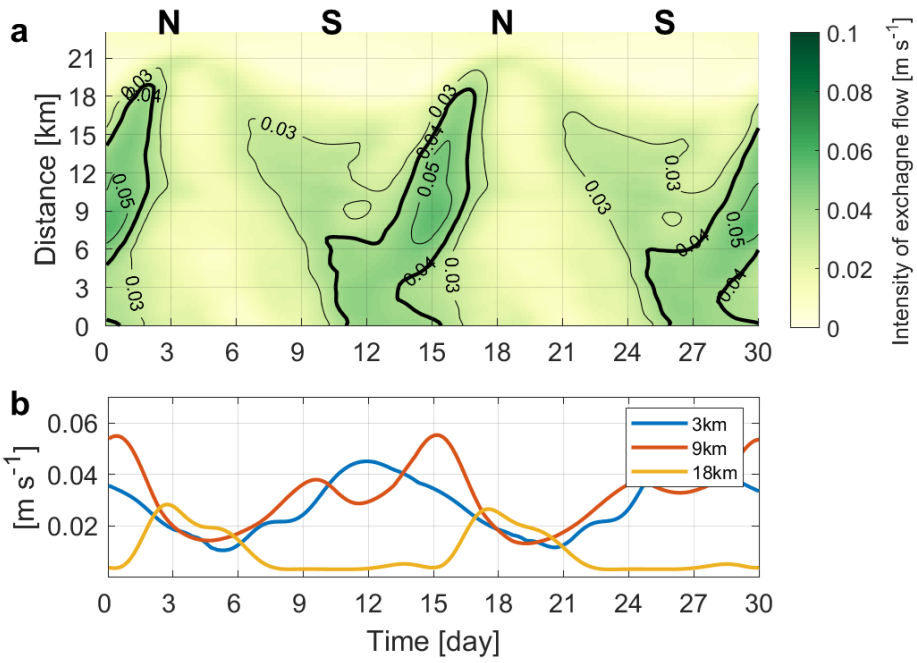

Figure 3.7 (a) Hovmöller diagram of the depth-averaged absolute value of the exchange flow and (b) timeseries of the intensity of the exchange flow at 3, 9, and 18 km from the estuary mouth (unit: m s^{-1}).

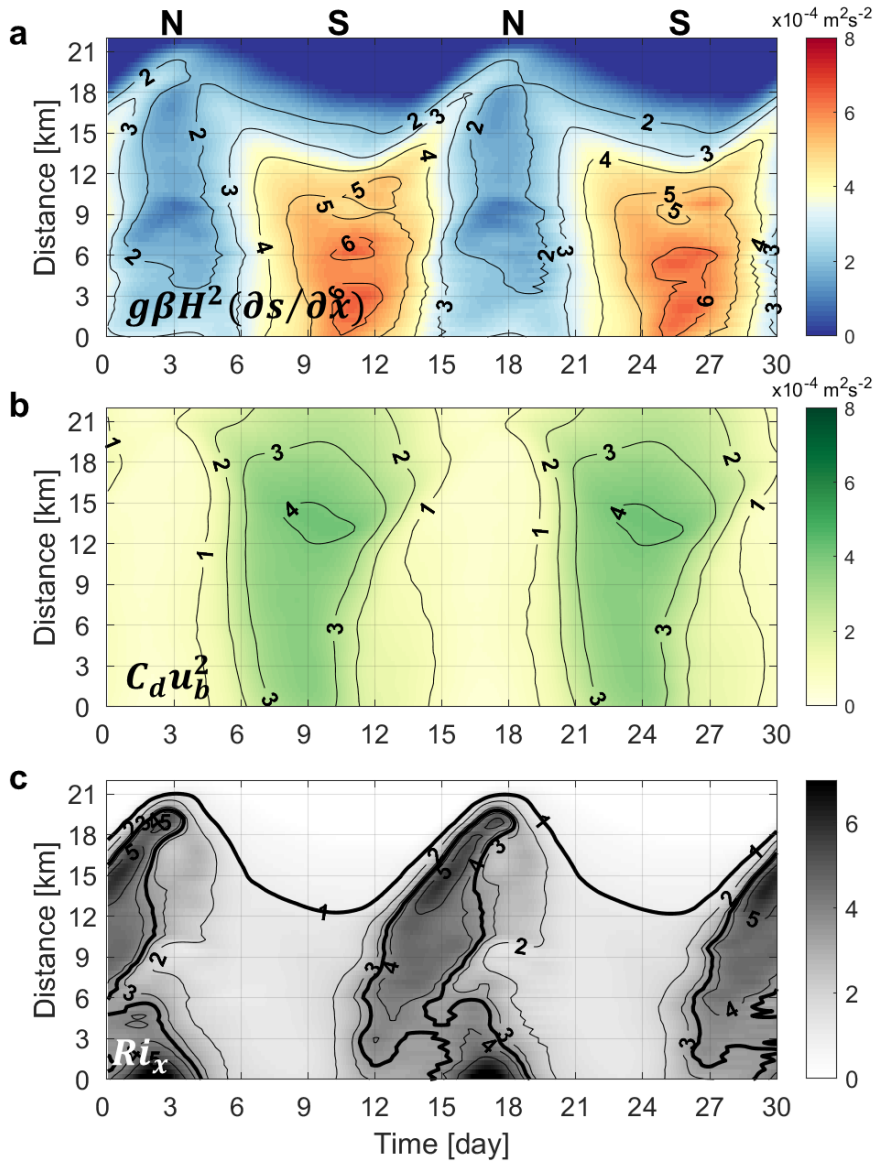

Figure 3.8 Hovmöller diagram of the (a) baroclinic forcing (unit: m^2 s^{-2}), (b) bottom stress (unit: m^2 s^{-2}), and (c) nondimensional horizontal Richardson number.

3.3.3. Restriction of salt intrusion by vertical mixing

Unlike many estuaries, in the Sumjin River estuary, the exchange was stronger during spring tide than during neap tide in the lower estuary. This was also confirmed through the idealized model experiment, and it was quantitatively proved with Ri_x that the salinity gradient effect was large enough to overwhelm the vertical mixing effect. In order for the salinity gradient to be sufficiently large during the spring tide, the response time of salinity distribution had to coincide with the timescale of variation in vertical mixing (Park and Kuo, 1996). As vertical mixing increased, the salinity gradient increased, which could be the maximum during spring tides. In particular, this phenomenon occurred in short estuaries rather than long estuaries where the timescale of mass response was long (Park and Kuo, 1996). I estimated the vertical eddy diffusivity of salt (K_s) to examine the intensity of vertical mixing, which was the most common approach for quantification of the mixing in estuaries (Fischer, 1972; MacCready, 2007). I selected the 5 $\mathrm{g\,kg^{-1}}$ isohaline of bottom salinity to represent the salt intrusion length (Figure 3.9). A scatter plot of the salt intrusion distinctly showed an inverse linear relationship between the isohaline length and K_s. During the spring

tide, when vertical mixing was strongest, the salinity gradient was at its maximum because the salt intrusion was at its minimum.

The relationship between exchange flow and salinity gradient concerning vertical mixing can be summarized as follows. As vertical mixing increased, the vertical shear of exchange flow decreased, and stratification weakened. As a result, F_E driving the landward salt flux decreased, and the total salt flux became seaward, resulting in salt intrusion that was shortened but vertically homogenous. During the spring tide, the salt intrusion was minimal, and the salinity gradient in the lower estuary was large (~ 2.3 g kg^{-1} km^{-1}); I found that it was 2-4 times larger than that of other longer estuaries (e.g., 1 g kg^{-1} km^{-1} in the Modaomen estuary [~ 63 km] and 0.6 g kg^{-1} km^{-1} in the Hudson River estuary [> 100 km]). The salinity gradient was large enough to overwhelm the vertical mixing effect, which intensified the vertical shear of exchange flow, resulting in the development of stratification. Therefore, as F_E increased, the total salt flux became landward. As the tidal range decreased, salt was imported into the estuary, and salt intrusion became longer. The strengthening of the convergence of the landward salt flux during this period induced the maximum salinity gradient to proceed further into the estuary. This process was repeated while the tidal range

decreased, such that the maximum salinity gradient at the head enhanced the exchange flow during the neap tide.

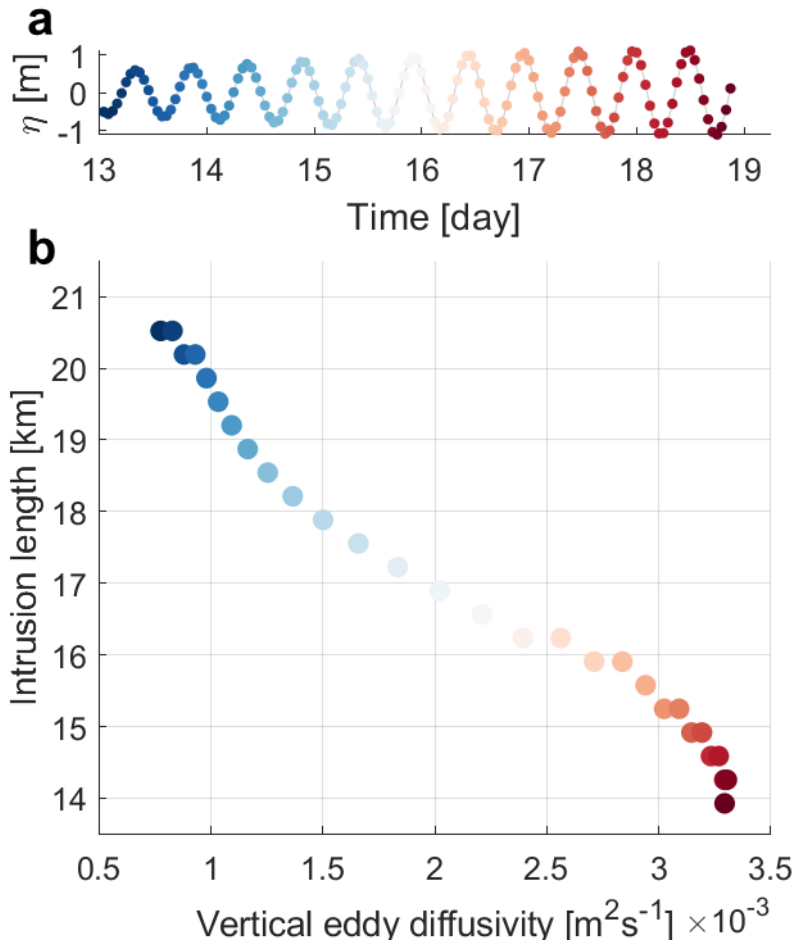

Figure 3.9 (a) Time series of sea-surface height (unit: m) and (**b**) scatter plot of intrusion length (unit: km) of the isohaline 5 versus cross-sectionally averaged vertical eddy diffusivity Ks (unit: $m^2\ s^{-1}$) from the model results. Each colored dot in (**b**) indicates each timing denoted by the same colored dot in (**a**).

3.3.4. Model application to realistic topography in the Sumjin River estuary

The idealized model clearly showed the variations of salinity gradient in the entire short estuary and its effect on the exchange flow over fortnightly tidal cycles. However, the idealized model should have considered the effect of complicated topography on variations in the salinity gradient and exchange flow. A numerical experiment with realistic topography was conducted to confirm the spatiotemporal variations of the salinity gradient and exchange flow in the Sumjin River estuary. The river discharge rate (30 $m^3 s^{-1}$) in 2013 was applied for the realistic model. Other model settings were the same as those used in the idealized model experiment.

The realistic model appropriately simulated the fortnightly variation in the depth-averaged salinity and the horizontal salinity gradient. The horizontal salinity gradient changed periodically over fortnightly tidal cycles as in the idealized model experiment, although its large value appeared sparsely owing to an uneven depth distribution (Figure 3.10). The occurrence of large horizontal salinity gradients may be attributed to the saline waters, which persist for a few days due to varying depths. The spatiotemporal change of

exchange flow corresponded well with that of the horizontal salinity gradient, which showed out of phase between lower and upper estuaries, as in the idealized model experiment.

Both idealized and realistic models showed a more significant salinity gradient and a more roubust exchange flow variation during the spring tide, which was consistent with the observations of Cho et al. (2020) in the lower estuary. However, the model results suggested that the salinity gradient was smaller and the exchange flow was weaker in the upper estuary during the spring tide. However, it was the opposite of that in the lower estuary.

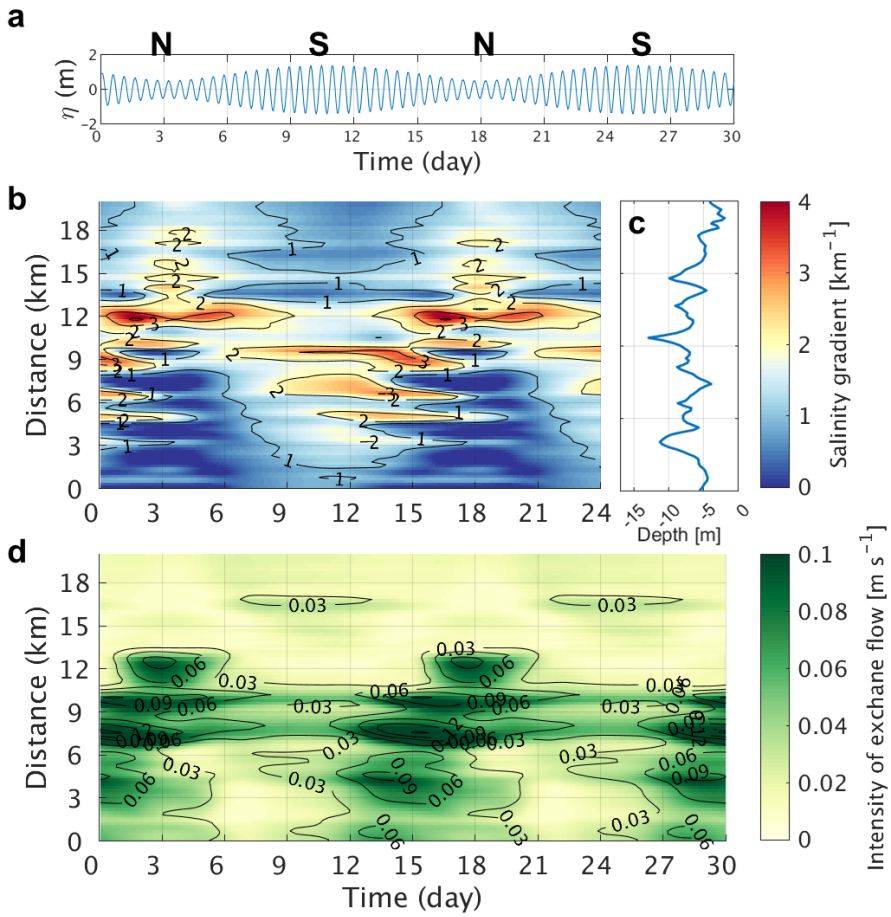

Figure 3.10 (a) Time series of sea-level height at the mouth of the real case and the N and S stand for neap tide and spring tide, respectively. Hovmöller diagram of (b) horizontal salinity gradient along the channel (unit: km^{-1}). (c) Depth variation in the Sumjin River estuary toward upstream, which is averaged across the channel (unit: m). (d) Hovmöller diagram of the depth-averaged absolute value of the exchange flow (unit: ms^{-1}).

3.4. Summary and Conclusion

Fortnightly variation of horizontal salinity gradient and exchange flow, and their mechanism, were investigated in an estuary with a short length and narrow width (i.e., the Sumjin River estuary). The fortnightly variation of the exchange flow had a different phase in the lower and upper estuary: in the lower estuary, it was strong during spring tides, but in the upper estuary, it was strong during neap tides.

Vertical mixing became weaker during transitions from spring to neap tides, and baroclinic forcing dominated owing to the maximum salinity gradient moving from the mouth to the head. This intensified the vertical shear of exchange flow and developed stratification, increasing the steady shear dispersion salt flux. Therefore, the total salt flux was landward, and the salt intrusion became longer. Where convergence was strong while the salt flux was landward, the salinity gradient was at a maximum, making the exchange flow stronger toward the inside of the estuary. The salt intrusion continued to lengthen, the salinity gradient at the head of estuary was maximized, and the exchange flow was also strong during neap tides. While the tidal range increased, vertical mixing became stronger throughout the estuary and more dominant than the baroclinic forcing effect,

resulting in weaker exchange flow and decreased landward salt flux. The total salt flux was seaward by the advective salt flux. As salt was exported out of the estuary, salt intrusion continued to be shortened. The salinity gradient increases in the lower estuary due to the minimum salt intrusion during the spring tide.

As vertical mixing decreased after the peak spring tide, baroclinic forcing became dominant, and the exchange flow began to intensify again. The salinity gradient was the determinant of the fortnightly variation of exchange flow in the entire estuary. The spatiotemporal change of strong exchange flow (> 0.04 m s^{-1}) corresponded well with that of a high Simpson number ($Ri_x > 3$). Owing to the change in the salt intrusion determined by vertical mixing, the maximum salinity gradient periodically reciprocated while the tidal range decreased; this dominated the vertical mixing effect, enhancing the exchange flow. Since the maximum salinity gradient was out of phase between the lower and upper estuaries, the phase of the exchange flow also varied depending on the location of the estuary.

Fortnightly variation in the salinity gradient and exchange flow also appeared in the model using realistic topography for the Sumjin

River estuary. However, the non-linear topographic effects disturbed the fortnightly oscillation of the maximum salinity gradient zone and the exchange flow. This study proposes that the observations at a specific point cannot represent the fortnightly variation in the horizontal salinity gradient and exchange flow. The spatiotemporal variation over the entire estuary should be investigated to understand the estuarine circulation in a short and narrow estuary like the Sumjin River estuary

4. Effect of river discharge on horizontal salinity gradient and exchange flow during fortnightly tidal cycle

4.1. Introduction

Estuaries vary greatly in size, shape, and forcing characteristics, but a general feature is the dilution of saline water with fresh water, resulting in a horizontal salinity gradient. The horizontal salinity gradient is a key driving force for estuarine exchange flow (Pritchard, 1967), determining the distribution and transport of suspended materials, such as pollutants and biota (Ahel et al., 1996; Blaise and Deleersnijder, 2008; Garel and Ferreire, 2013; Toublanc et al., 2015). The horizontal salinity gradient is induced and sustained by river inflow (Kraneburg, 1986; Restrepo and Kjerfve, 2002), although its magnitude is dependent on the river inflow rate and tidal mixing (MacCready, 2007).

There have been various studies on horizontal salinity gradients and exchange flow based on observations and model experiments. Some of these studies assumed that the horizontal salinity gradient was spatially uniform and invariant with time (Simpson et al., 1990;

Sharples and Simpson, 1993; Monismith and Fong, 1996). This could be attrributed to the limitations of the observational data and efficiency of the model (lower Hudson River estuary - Geyer et al., 2000). Subsequent studies considered a simple time-dependent salinity gradient (Warner et al., 2005; Blaise and Deleersnijder, 2008). However, these unrealistic parameterizations were unable to explain the dynamic variations associated with the horizontal salinity gradient. Comparisons between observations and model results often indicated serious discrepancies or brought indefinite increase in stratification (run-away stratification) (Sharples and Simpson, 1993; Monismith et al., 1996).

Recently, few studies suggested that the horizontal salinity gradient may fluctuate with river flow (Kranenburg, 1986; Geyer et al., 2000; Restrepo and Kjerfve, 2002; Warner et al., 2005; Chua, 2013) and tide (Ralston and Geyer, 2008). As the river flow increased, the local salinity gradient at the mouth of the estuary had to increase to compensate for the decrease in salt intrusion length (Warner et al., 2005). More substantial vertical mixing induced by tide intensified the horizontal salinity gradient by stimulating the vertical movement of momentum and tracer, allowing fresher water to reach the lower portion of the water column (Becker et al., 2010).

Weak vertical mixing activated the horizontal movement of salt, strengthening the stratification and reducing the salinity gradient.

However, studies analyzing changes in horizontal salinity gradients in the entire estuary by considering variations in river flow and tidal mixing are insufficient. In the Hudson River estuary, one of the longest estuaries, a spring–neap variation in salinity gradient was reported with river discharge. During the period of low river discharge, the salinity intrusion of the Hudson displayed little changes over spring–neap cycles; therefore, the salinity gradient hardly changed (Bowen and Geyer, 2003; Lerczak et al., 2009). However, the salinity gradient had significant spring–neap variability during the higher discharge period (Ralston et al., 2008). Afterward, Geyer and Ralston (2015) implemented a salinity gradient under a constant river discharge rate through a numerical model experiment. However, because the study focused on frontogenesis by local enhancement of salinity gradient, the mechanism of change in salinity gradient or its effect on exchange flow could not be analyzed. Even in short estuaries, little is known about changes in the salinity gradient with forcings such as river flow and tide in the entire estuary.

In this study, the variability of salinity gradient according to river

discharge rate during the fortnightly tidal cycle and its effect on the exchange flow were investigated in the short Sumjin River estuary. For this, a validated 3-D numerical model was used, and the physical process of salt transport was analyzed through the salt flux decomposition method. This study proposes the relationship between the change in salinity structure, the associated mechanisms, and circulation under various forcing situations in a short estuary such as the Sumjin River estuary.

4.2. Materials and Methods

4.2.1. Model description

In this numerical study, the Regional Ocean Modeling System (ROMS: Shchepetkin and McWilliams, 2005; Haidvogel et al., 2000) was used to simulate an idealized Sumjin River estuary. ROMS solves the hydrostatic, incompressible, Reynolds-averaged momentum and tracer conservation equations with a terrain-following vertical coordinate and free surface. The topography was simplified to focus only on changes in salinity structure due to tidal amplitude and river discharge rate. Salinity structure could be reproduced well for various forcing by showing a spatio-temporal change similar to the salt distribution of the model to which the actual topography was applied in chapter 3.

The bay length was 7 km, and the estuarine channel length was 25 km (Figure 1b, c). The cross-section was rectangular in shape, and the water depth and width followed a linear trend based on the actual change. The grid configuration was 110 (along-channel, y-direction) by 17 (cross-channel, x-direction) grids by 10 (vertical levels). The model grid had along-channel grid resolution in the range of 10 – 540 m and cross-channel resolution in the range of

6 – 240 m.

The model was forced by M_2 and S_2 tidal constituents from the southern boundary and a constant freshwater flux from the river end.

The minimum river flow rate was set tp 10 m^3s^{-1}, and a total of 13 cases were perdormed by increasing the flow rate from 20 to 240 m^3s^{-1} at 20 m^3s^{-1} intervals These river flow rates cover low to high discharge conditions, with 80 m^3s^{-1} representing the monthly mean. The temperature was fixed at 20 ℃ throughout the domain. Salinity at the river end was set to 0 g kg^{-1}, whereas at the southern boundary salinity was an oceanic value of 35 g kg^{-1}. The turbulence closure scheme used was the K-Profile Parameterization scheme (KPP; Large et al., 1994). The southern boundary was treated with the Champman condition for surface elevation, Flather condition for barotropic velocity, and Clamped boundary conditions for open-ocean salinity. The idealized model was integrated for 100 days with a baroclinic time step of 10 s. After the salt structure reaches a steady state, numerical experiments were performed to investigate the effect of changing river discharge rate and tidal amplitude. The idealized model presented a steady spring-neap tidal cycle in the salinity field after a spin-up period of 30 days, after which it was run

for another 70 days to capture several fortnightly tidal cycles.

4.3. Results

4.3.1. Fortnightly variation of horizontal salinity gradient according to river discharge

The spring–neap variation of salinity distribution and horizontal salinity gradient were analyzed as a function of river discharge and tidal mixing. Depending on the river discharge rate, the subtidal salinity and maximum horizontal salinity gradient changed differently (Figure 4.1) during the spring–neap tidal cycle (Figure 4.1a).

Under low discharge conditions (Figure 4.1b,e), the temporal change of salt distribution was different from the spring–neap tidal cycle. The salt intrusion was at its maximum during the neap tide, but the minimum occurred about 3 days before the peak neap tide. The inflow of hypersaline water was prolonged, and the water mass with a salinity of 27 or more advanced up to the middle estuary (approximately 10 km) regardless of the tidal range. Therefore, the difference in horizontal salinity from the mouth to middle estuary was insignificant. However, the horizontal difference in salinity caused the horizontal salinity gradient to be larger than in the lower or middle estuaries during both spring and neap tides. The maximum salinity

gradient occurred at the head of estuary during the neap tide.

During mean discharge conditions (Figure 4.1c, f), the change in the salt distribution became similar to the spring–neap tidal cycle. The salt intrusion length was still at its maximum during the neap tide but became minimal during the spring. As the distance of salt intrusion decreased significantly during spring tides rather than during neap tides, the horizontal difference of salinity in the lower and middle estuary increased. Therefore, the salinity gradient increased in the lower and middle estuaries. However, because the salt intrusion length remained long during neap tides, the horizontal salinity difference was greatest in the upper estuary, causing the horizontal salinity gradient to its maximum value.

During high discharge conditions (Figure 4.1d, g), the salt distribution changed according to the spring–neap tidal cycle and was symmetrical. These symmetrical changes were similar to that during the mean discharge condition. However, the salt intrusion length was shorter, and the salinity gradient increased. During the spring tides, the salinity gradient in the middle estuary increased by about 0.5 km^{-1} or more compared with that observed under the mean–discharge condition. During the neap tides, the salinity gradient was still high in

the upper estuary.

The spatial difference of the salinity gradient between the lower and upper estuaries became larger as the river discharge rate increased. Therefore, the spatial variations of horizontal salinity gradient during spring and neap tides were compared under various river discharge conditions (Figure 4.2). The spatial response of salinity gradient according to river discharge was stronger during the spring tide than during the neap tide. The spatial change was noticeable under the low to mean discharge conditions. During the spring tide, the salinity gradient decreased to zero in the upper estuary and increased by about four folds around the estuary mouth. The maximum salinity gradient moved from 17 km with the low discharge rate to 11 km with the mean discharge rate. It generally reached its maximum in the upper estuary during the neap tide. There was only a slight shift in the position where the maximum value appeared as the river discharge increased.

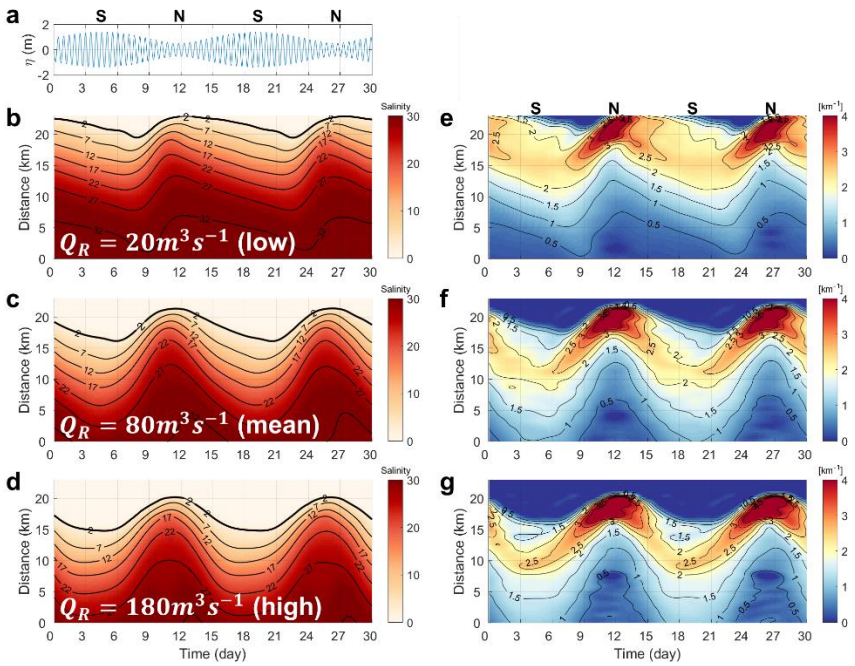

Figure 4.1 (A) Time series of sea-level height at the mouth of the idealized estuary and the N and S stand for neap tide and spring tide, respectively. Hovmöller diagrams of the (b, c, d) sectionally averaged subtidal salinity and (e, f, g) horizontal salinity gradient along the channel (unit: km^{-1}) during (b, e) low, (c, f) mean, and (d, g) high discharge conditions. S and N denote spring and neap tide, respectively.

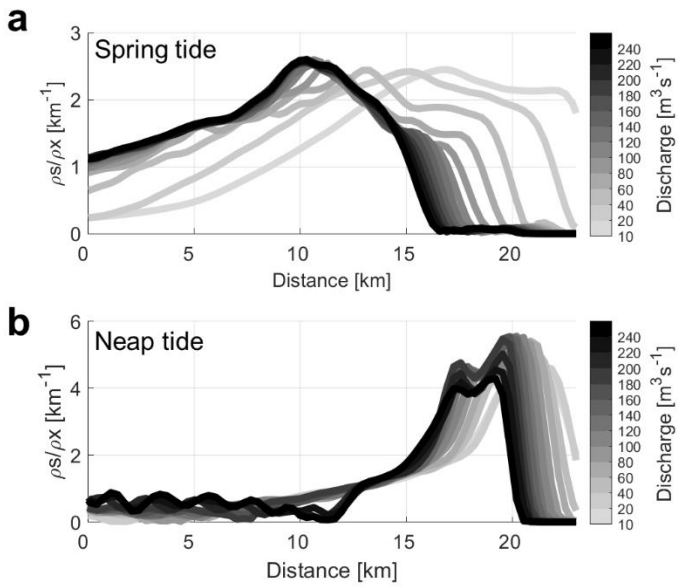

Figure 4.2 Along channel salinity gradient (unit: km^{-1}) during (a) spring and (b) neap tides based on the river discharge rate. The darker the curve, the higher the river dischrge rate.

4.3.2. Exchange flow according to river discharge

Exchange flow generally became stronger as the river discharge rate increased and displayed interesting spatiotemporal changes. To calculate the intensity of the exchange flow, the absolute value of the exchange flow was vertically integrated (Figure 4.3). At the intensity $\geq$ 0.04 (unit: ms^{-1}), the exchange flow can be set as strong because, at this intensity, F_E due to the exchange flow can induce the total salt flux landward. With this criterion, the main factor determining the fortnightly variation in the strength of the exchange flow depends on the river discharge. As indicated in the previous chapter, during mean discharge conditions, the spring–neap variation of the exchange flow between the lower and upper estuaries was out of phase. However, as the discharge rate was changed, the spatiotemporal distribution of the exchange flow also changed.

During low discharge conditions, the exchange flow was weak during the spring tide but uniformly strong along the channel during the neap tide. These changes were similar to the results presented in several other studies on estuaries; including the Hudson River estuary (Bowen and Geyer, 2003), Modaomen estuary (Gong et al., 2014), Suisun Bay in San Francisco Bay (Stacey et al., 2010), the

Satilla River estuary (Blanton et al., 2003), and the CAMBORIÚ ESTUARY, BRAZIL (Siegle et al., 2009). In these studies, the exchange flow was stronger during neap tides than during spring tides. However, when the river discharge rate was above the mean, the exchange flow became stronger even during the spring tide in the lower estuary compared with that observed in the case of low discharge. This change was similar to the salt flux conversion to landward during spring tides as the river discharge rate increased, as shown in section 4.3.3.

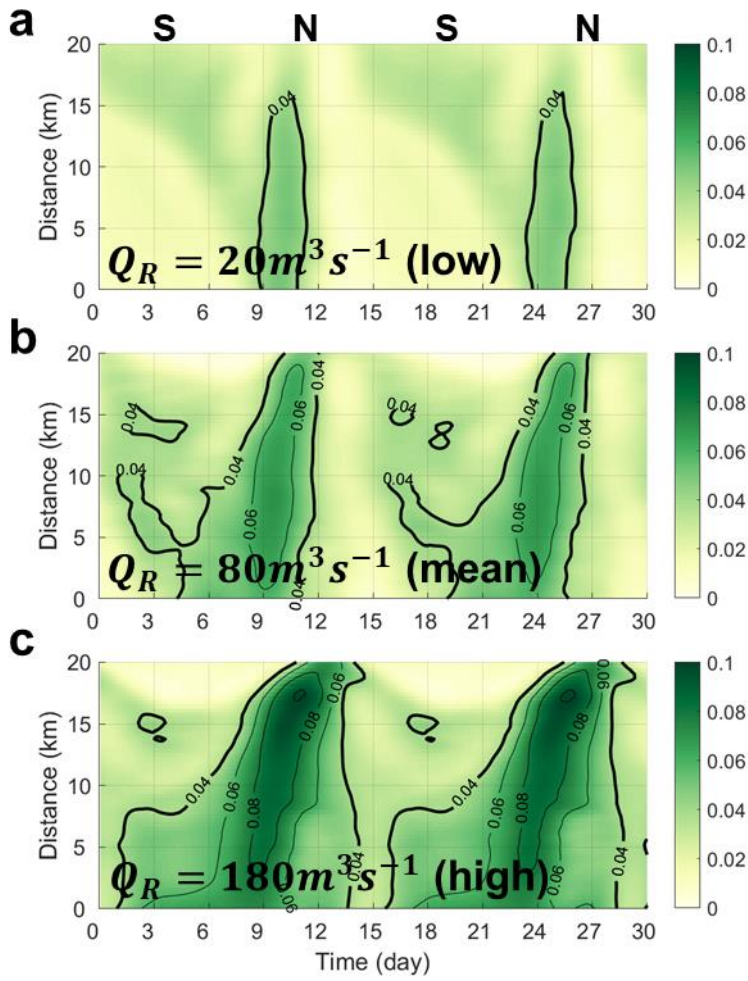

Figure 4.3 Hovmöller diagrams of the intensity of exchange flow (unit: ms^{-1}) during low, mean, and high discharge conditions. S and N denote spring and neap tide, respectively.

4.3.3. Physical process of salt flux

The spatiotemporal distribution of salt and salinity gradient that varied with discharge rate and tidal mixing were determined by salt flux. To find out the detailed physical process for salt transport, the salt flux were divided into three mechanisms by applying the salt flux decomposition method proposed by Lerczak et al. (2006),

$$\boldsymbol{F = F_R + F_E + F_T,} \tag{4.4}$$

where F_R is the advective salt flux, F_E is the steady shear dispersion salt flux, and F_T is the tidal oscillatory salt flux.

The contribution of the salt flux to seaward was the advective salt flux (F_R) by river flow. The landward salt flux was induced by the steady shear dispersion salt flux (F_E) due to the exchange flow ,and the tidal oscillatory salt flux (F_T). The diffusive fraction ($\nu = F_T/(F_T + F_E)$), confirmed that the contribution of steady shear dispersion to the landward salt flux was higher ($\nu < 0.5$) during two fortnightly tidal cycles. In particular, since F_E contributed more than 75% of the total landwaard salt flux, the landward salt flux was determined by F_E. Therefore, this study area can be regarded as an F_E dominated estuary (Banas et al., 2004). The results showed that

the main mechanism of total salt flux were F_R and F_E.

As river discharge increased, both F_R and F_E increased (Figure 4.4). F_R varied according to the period of the spring–neap tidal cycle, and the seaward salt flux induced by F_R was stronger during the neap tide than during the spring tide (Figure 4.4a, b, c). F_E had higher spatial variability with increasing river discharge rate than F_R. During low discharge conditions, F_E was strong throughout the estuary only during the neap tide (Figure 4.4d, e, f). But as the discharge rate increased, the time of F_E strengthening in the lower estuary advanced. Even during the spring tide, F_E became strong in the lower estuary during high discharge conditions. The change in F_E was related to the advance in the transitions of total salt flux from seaward to landward (Figure 4.4g, h, i).

As the river discharge increased, the seaward of total salt flux increased and the duration time was shortened, whereas the landward of total salt flux increased, but the duration time increased. Based on the estuary mouth, the timing when the salt flux was converted to the landward under low discharge conditions was on day 9, and it closed to the neap tide. However, the conversion occurred on day 6 under mean discharge conditions and on day 4 under high discharge

conditions. It was getting closer to the spring tide.

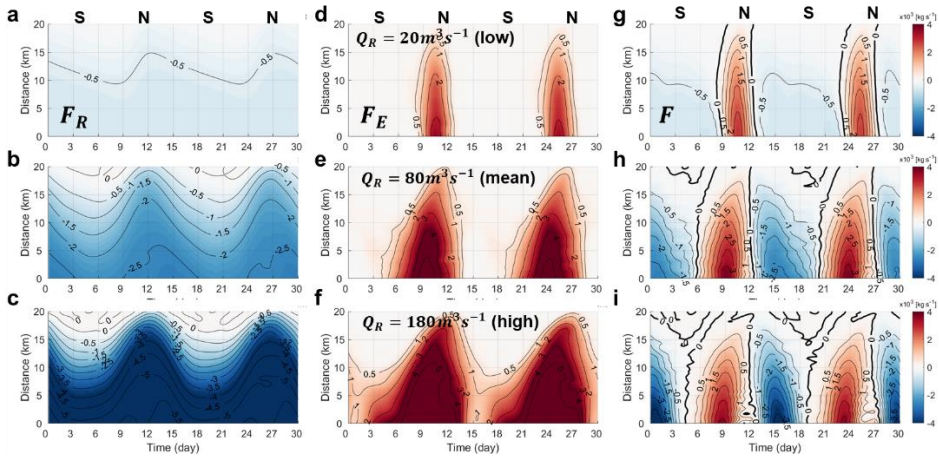

Figure 4.4 Hovmöller diagrams of (a, b, c) advective salt flux (F_R), (d, e, f) steady shear dispersion salt flux (F_E), and (g, h, i) total salt flux (F) during (a, d, g) low discharge, (b, e, h) mean discharge, and (c, f, i) high discharge conditions (unit: kg s^{-1}). S and N denote spring and neap tides, respectively.

4.4. Discussion

The spring–neap response of the horizontal salinity gradient became more pronounced as the river discharge rate increased. This was related to the advance of the conversion time of the salt flux. Moreover, this changed not only the spatiotemporal change in exchange flow but also the main determinant of spring–neap variation.

4.4.1. Difference between salt inflow and outflow according to river discharge

The total salt flux was seaward by F_R. As the river discharge rate increased from 20 m^3s^{-1} to 180 m^3s^{-1}, the seaward volume flux due to the river–induced barotropic flow increased by nine flods. In contrast, the subtidal salinity (based on the middle estuary - 12km from the mouth) decreased by half. Because the increase in seaward volume flux was greater than the decrease in subtidal salinity, F_R eventually increased. In particular, while the tidal range increased, F_R played a leading role in salt transport because the exchange flow was weakened by strong vertical mixing, which caused a reduction in F_E. The salt intrusion length became shorter as the salt outflow

continued through F_R. As the river discharge rate increased, the salt intrusion length shortened, and the horizontal salinity difference decreased, eventually increasing the salinity gradient.

After peak spring tide, the vertical mixing decreased as the tidal range decreased (Figure 4.5d, e, f). However, the baroclinic forcing induced by the salinity gradient was strong enough to overwhelm the vertical mixing effect (Figure 4.5 a, b, c). Consequently, exchange flow became stronger during both spring and neap tides (Figure 4.6). When the river discharge was high, the salt intrusion length was further reduced, increasing the salinity gradient in the lower estuary but weakening vertical mixing. Relatively, the baroclinic forcing was further strengthened, and the vertical shear of exchange flow was more emphasized, which intensified the landward salt flux. Therefore, when the river discharge rate was high, the seaward volume flux increased while the tidal range increased, resulting in a large salt outflow. On the contrary, when the tidal range decreased, salt inflow by exchange flow was largely due to strong baroclinic forcing caused by the salinity gradient.

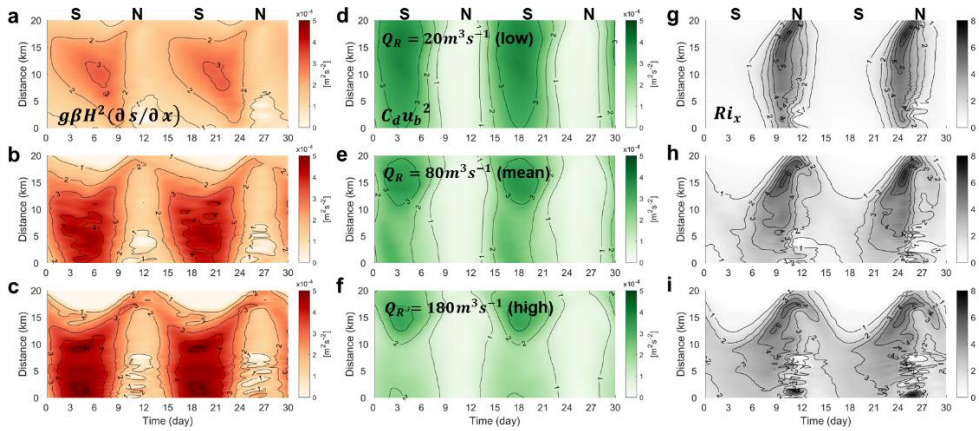

Figure 4.5 Hovmöller diagrams of the (a, b, c) baroclinic forcing (unit: m2 s−2), (d, e, f) bottom stress (unit: m2 s−2), and (g, h, i) nondimensional horizontal Richardson number during (a, d, g) low discharge, (b, e, h) mean discharge, and (c, f, i) high discharge conditions.

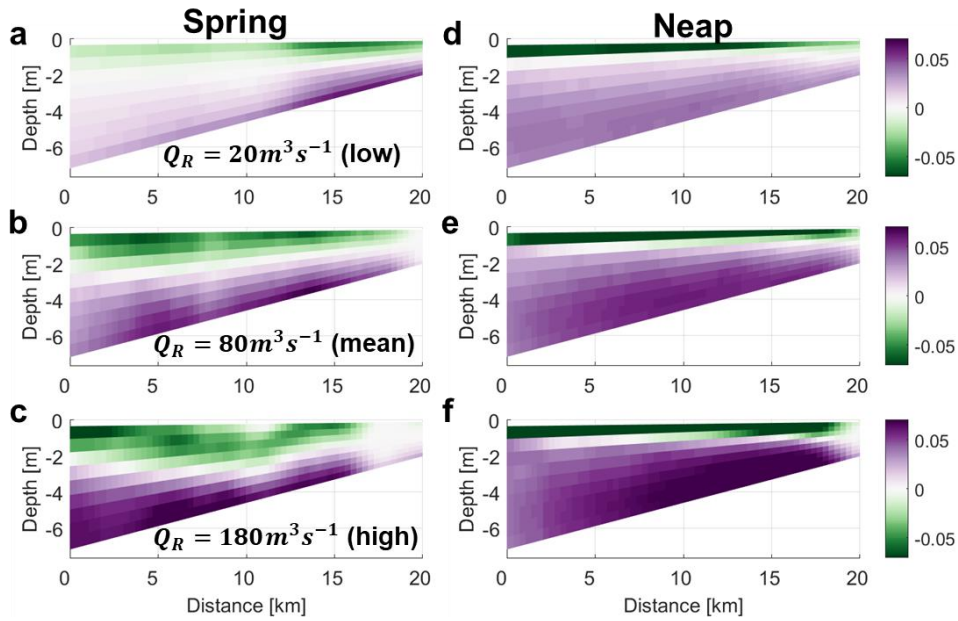

Figure 4.6 Vertical section of along−channel exchange flow (unit: m s^{-1}) during (a, b, c) spring and (d, e, f) neap tide during (a, d) low discharge, (b, e) mean discharge, and (c, f) high discharge conditions.

4.4.2. Advance of salt flux conversion time according to river discharge rate

As river discharge increased, the transition of salt flux from seaward to landward advanced to the spring tide. The salt intrusion length was shortest when the salt flux was converted from seaward to landward, and it was longest when the salt flux was converted in the opposite direction. The salt intrusion length based on isohaline 2 was greatest during neap tides, regardless of the river discharge rate. However, the minimum salt intrusion length was observeed on day 8 during low discharge conditions, but it approached the spring tide on day 4 during high discharge conditions.

As the river discharge increased, the salinity gradient became progressively larger during the spring tide, while the vertical mixing weakened overall. For example, during low to high discharge rate, the baroclinic forcing induced by the salinity gradient increased by more than two folds (Figure 4.5a, b, c), while the intensity of vertical mixing was reduced by roughly one− third (Figure 4.5d, e, f). Ri_x is the horizontal Richardson number, which is the a result of the competition between baroclinic forcing and vertical mixing (Figure 4.5g, h, i).

$$Ri_x = \frac{g\beta H^2(\partial s/\partial x)}{C_d {u_b}^2} \quad (4.5)$$

where β is the saline contraction coefficient, g is the acceleration due to gravity, $\partial s/\partial x$ is the horizontal salinity gradient, H is the local water depth, C_d (4.0×10^{-3}) is the drag coefficient (used in the model setting), and u_b is the amplitude of the bottom tidal velocity (Stacey et al., 2001). If the horizontal Richardson number is greater than 1, baroclinic forcing is dominant, and if it is greater than 3, it means that the exchange flow can be strong enough to increase the steady shear dispersion salt flux. In the lower estuary, when Ri_x became more than 3 or more, it was around day 9 during low discharge conditions, but it gradually approached the spring tide with day 6 and 4 during mean and high discharge conditions, respectively. This indicated that as the river discharge increased, the time for the onset of the effect of baroclinic forcing, which was large enough to overwhelm vertical mixing, became faster. Moreoveer, as the river discharge rate increased, the exchange flow during the spring tide became stronger, and steady shear dispersion played a major role in salt flux; hence, the conversion of salt flux to landward advanced to the spring tide.

4.4.3. Change of determinant of fortnightly variation of exchange flow

To calculate the intensity of the exchange flow, the absolute value of the exchange flow was vertically integrated (Figure 4.9). If the intensity was 0.04 or more (unit: ms^{-1}), the exchange flow could be set as strong because, at this intensity, F_E due to the exchange flow can induce the total salt flux landward. With this criterion, the main factor determining the fortnightly variation in the strength of the exchange flow depended on the river discharge.

Vertical mixing determined the spring–neap variation of exchange flow during low discharge conditions. During the spring tide, the exchange flow was weak, but it was uniformly strong along the channel during the neap tide. These changes are similar to the results presented in many other estuary studies; the Hudson River estuary (Bowen and Geyer, 2003), the Modaomen estuary (Gong et al., 2014), Suisun Bay in San Francisco Bay (Stacey et al., 2010), the Satilla River estuary (Blanton et al., 2003), and the CAMBORIÚ ESTUARY, BRAZIL (Siegle et al., 2009). These study found that the strong exchange flow matched the spatiotemporal pattern with weak vertical mixing ($< 1\ m^2 s^{-2}$).

The salinity gradient was generally low during low discharge condition, except in the upper estuary, so baroclinic forcing was weak. On the other hand, the vertical mixing effect determined the spatiotemporal change of the vertical shear of exchange flow because it was intense. This was supported by the fact that Ri_x was greater than 3, and the intensity distribution of vertical mixing was the opposite. As a result, during low discharge conditions, the fortnightly variation of exchange flow was determined by changes in the intensity of vertical mixing.

However, above the mean river discharge rate, the salinity gradient with a distinct spring–neap variation determines the spring–neap change in exchange flow. Compared with that observed during the low discharge condition, the exchange flow was generally more substantial, and in the lower estuary, it was strong even during the spring tide with high vertical mixing. While the tidal range decreased, the exchange flow became more robust inside the estuary. The spatiotemporal change of strong exchange flow was comparable to the change when the effect of baroclinic forcing had a more significant impact than vertical mixing (Ri_x >3). As the flow rate increased, the salinity gradient increased due to the shortened salt inflow distance. In particular, the increase in the lower estuary was noticeable during

the spring tide, which allowed the effect of baroclinic forcing to overwhelm that of vertical mixing, and consequently the exchange flow was strengthened.

4.5. Summary and Conclusion

In the Sumjin River estuary, the response to the fortnightly tidal cycle of salinity gradient and exchange flow varied depending on the river discharge rates. During low discharge rates, the response to the spring–neap tidal cycle of the salt distribution was not evident. However, as the river discharge rate increased, the periodic response of salt intrusion and salinity gradient became stronger. While the tidal range increased, salt outflow increased due to the increased seaward volume flux induced by the river discharge rate. The salt intrusion length became shorter, and there was a reducton in the salinity gradient in the lower estuary during the spring tide. The high salinity gradient enhanced the exchange flow, and the salt flux began to go landward by steady shear dispersion. Consequently, the increase in river flow rate strengthened the exchange flow even when the tidal range was high, thereby advancing the onset of landward salt flux. In addition, as the river flow rate increased, the exchange flow from the effect of baroclinic forcing became stronger; hence, not only the seaward salt flux but also the landward salt flux was high.

The primary factor influencing the fortnightly variation of exchange flow changed in response to salt distribution according to

river discharge rate. With a low river discharge rate, vertical mixing was the dominant factor, and when the river discharge rate increased, the baroclinic forcing induced by the salinity gradient became the main factor. Because as the river discharge increased, the spring-neap variation of salinity gradient also became more pronounced, primarily due to the effect of the high salinity gradient in the lower estuary during the spring tide.

The length of estuary must be short for the salinity gradient to be large enough to drive a fortnightly variation of exchange flow. This was supported by the short distance between the mouth of estuary and the river source point and the short salt intrusion induced by high river flow rate also exerted a similar effect. In the future, if the response to various external forcings, such as a sea-level rise or atmospheric heat, is analyzed for different estuary lengths, as the results would facilitate the establishment of strategies that 추 be adopted improve circulation throughout the estuary.

5. Summary and Conclusions

This study investigated the spring–neap variation of salinity gradient and exchange flow according to river discharge and tidal mixing. The change mechanism of the salinity gradient and its effect on the exchange flow were analyzed in the short Sumjin River estuary. In the observational results, the exchange flow in the lower estuary was strong during the spring tide and weak during the neap tide, unlike other estuaries. It was found that the spring–neap variation was caused by the horizontal salinity gradient through the analytical model. Since the Sumjin River estuary is short, the salinity gradient that maximizes during the spring tide was large enough to enhance the exchange flow. A numerical model was used to analyze whether this unique change was limited to a specific point or a characteristic of the entire estuary. Overcoming the limitations of location and time by observation, I focused on the spring–neap variation of exchange flow in the entire estuary. The fortnightly variation of exchange flow was different between lower and upper estuaries. Exchange flow was strong during the spring tide only in the lower estuary and weaker in the upper estuary. This was due to a salinity gradient. The salinity gradient was maximal in the lower estuary during the spring tide,

progressed inward to the estuary during the decreasing tidal range, and was maximal at the head of estuary during the neap tide. While the tidal range decreased, the baroclinic forcing effect by the salinity gradient was more dominant than the vertical mixing, affecting the spatiotemporal distribution of the exchange flow.

Since the estuary is located in various river discharge conditions, the relationship between the spring–neap variation of the salt distribution and the exchange flow was analyzed using a numerical model from low to high discharge rates. As the river discharge rate increased, the salt distribution responded strongly to the spring–neap tidal cycle. In particular, the time when the salt intrusion length becomes minimum has been advanced to the spring tide. The contrast between landward and seaward salt flux also increased. Because the amount of salt outflow by seaward salt flux increases, the salt intrusion length becomes shorter, and the salinity gradient increases, strengthening the exchange flow and increasing the amount of salt inflow. The main factor determining the spring–neap variation of exchange flow also varied with the river discharge rate. During lower discharge, it is varied by vertical mixing and, when the flow rate increases, by salinity gradient.

Assuming that other conditions are similar, the shorter the estuary length, the shorter the range of salinity distribution along the channel, and thus the larger the salinity gradient. The unique spring–neap variation of the exchange flow in the Sumjin River estuary was because the salinity gradient was maximum during the spring tide, and the value was large enough to intensify the exchange flow. However, when the discharge rate is very low, the exchange flow becomes stronger only during the neap tide, as is the case for many other estuaries, because the salt intrusion length is relatively long even for short estuaries, reducing the salinity gradient. On the other hand, as the discharge rate increased, the salt intrusion length became shorter, so the spatiotemporal distribution of the exchange flow changed due to the increased salinity gradient. Even if the size of the estuary is small, the change in salt distribution reacts strongly to the spring–neap tidal cycle, and a river flow rate above a specific value is required to determine the change of exchange flow by the salinity gradient. Even in short estuaries, whether the salinity gradient played a dominant role in the fortnightly variation in exchange flow depends on the river flow rate.

Studies on changes in estuarine exchange flow due to sea–level rise or atmospheric heat related to global warming have been

conducted mainly in large-scale estuaries. However, in the future, detailed analyzes and studies are needed even in short estuaries such as the Sumjin River estuary.

References

Andutta, F. P., de Miranda, L. B., Franca Schettini, C. A., Siegle, E., da Silva, M. P., Izumi, V. M., & Chagas, F. M. (2013). Temporal variations of temperature, salinity and circulation in the peruipe river estuary (nova vicosa, ba). Continental Shelf Research, 70, 36-45. doi:10.1016/j.csr.2013.03.013

Baek, S. H., Seo, J.-Y., & Choi, J.-W. (2015). Growth characteristics and distribution pattern of a brackish water clam, corbicula japonica along an estuarine salinity gradient in seomjin river. Journal of the Korea Academia-Industrial cooperation Society, 16(10), 6852-6859. doi:10.5762/kais.2015.16.10.6852

Banas, N. S., Hickey, B. M., MacCready, P., & Newton, J. A. (2004). Dynamics of willapa bay, washington: A highly unsteady, partially mixed estuary. Journal of Physical Oceanography, 34(11), 2413-2427. doi:10.1175/jpo2637.1

Becker, M. L., Luettich, R. A., & Seim, H. (2009). Effects of intratidal and tidal range variability on circulation and salinity structure in the cape fear river estuary, north carolina. Journal of Geophysical Research, 114(C4). doi:10.1029/2008jc004972

Bowen, M. M., & Geyer, W. R. (2003). Salt transport and the time-dependent salt balance of a partially stratified estuary. Journal of Geophysical Research: Oceans, 108(C5). doi:10.1029/2001JC001231

Burchard, H., Hetland, R. D., Schulz, E., & Schuttelaars, H. M. (2011). Drivers of residual estuarine circulation in tidally energetic estuaries: Straight and irrotational channels with parabolic cross section. Journal of Physical Oceanography, 41(3), 548-570. doi:10.1175/2010jpo4453.1

Chen, S.-N. (2015). Asymmetric estuarine responses to changes in river forcing: A consequence of nonlinear salt flux. Journal of Physical Oceanography, 45(11), 2836-2847. doi:10.1175/jpo-d-15-0085.1

Chen, S.-N., Geyer, W. R., Ralston, D. K., & Lerczak, J. A. (2012). Estuarine exchange flow quantified with isohaline coordinates: Contrasting long and short estuaries. Journal of Physical Oceanography, 42(5), 748-763. doi:10.1175/jpo-d-11-086.1

Cho, E.-B., Cho, Y.-K., & Kim, J. (2020). Enhanced exchange flow during spring tide and its cause in the sumjin river estuary, korea. Estuaries and Coasts, 43(3), 525-534.

doi:10.1007/s12237-019-00636-9
Cronin, L. E., & Neilson, B. J. (1981). Estuaries and nutrients: Humana Press.
Dalrymple, R. W., Zaitlin, B. A., & Boyd, R. (1992). Estuarine facies models: Conceptual basis and stratigraphic implications: Perspective. Journal of Sedimentary Research, 62(6).
de Miranda, L. B., Bérgamo, A. L., & de Castro, B. M. (2005). Interactions of river discharge and tidal modulation in a tropical estuary, ne brazil. Ocean Dynamics, 55(5-6), 430-440. doi:10.1007/s10236-005-0028-z
Defant, A. (1960). Physical oceanography; volume 2. Pergamon Press, Oxford, 598.
Dijkstra, Y. M., Schuttelaars, H. M., & Burchard, H. J. J. o. G. R. O. (2017). Generation of exchange flows in estuaries by tidal and gravitational eddy viscosity-shear covariance (esco). 122(5), 4217-4237. doi:10.1002/2016JC012379
Dyer, K. (1973). Estuaries: A physical introduction. John wiley. In: London.
Dyer, K. (1974). The salt balance in stratified estuaries. Estuarine and coastal marine science, 2(3), 273-281.
Dyer, K. (1997). Partially mixed and well-mixed estuaries. Estuaries—a physical introduction. 136-164.
Fischer, H. (1972). Mass transport mechanisms in partially stratified estuaries. Journal of fluid mechanics 53(4), 671-687. doi:10.1017/S0022112072000412
Fischer, H., List, E., Koh, R., Imberger, J., & Brooks, N. (1979). Mixing in estuaries. Mixing in Inland and Coastal Waters, 229-278.
Garcia, A. M. P., Geyer, W. R., & Randall, N. (2022). Exchange flows in tributary creeks enhance dispersion by tidal trapping. J Estuaries Coasts 45(2), 363-381. doi:10.1007/s12237-021-00969-4
Garel, E., & Ferreira, O. (2013). Fortnightly changes in water transport direction across the mouth of a narrow estuary. Estuaries and Coasts, 36(2), 286-299. doi:10.1007/s12237-012-9566-z
Garvine, R. W. (1985). A simple model of estuarine subtidal fluctuations forced by local and remote wind stress. Journal of Geophysical Research: Oceans, 90(C6), 11945-11948.
Geyer, W., & Cannon, G. (1982). Sill processes related to deep water renewal in a fjord. Journal of Geophysical Research: Oceans,

87(C10), 7985-7996.
Geyer, W. R., & MacCready, P. (2014). The estuarine circulation. Annual Review of Fluid Mechanics, 46(1), 175-197. doi:10.1146/annurev-fluid-010313-141302
Geyer, W. R., & Ralston, D. K. (2015). Estuarine frontogenesis. Journal of Physical Oceanography, 45(2), 546-561. doi:10.1175/jpo-d-14-0082.1
Geyer, W. R., Trowbridge, J. H., & Bowen, M. M. (2000). The dynamics of a partially mixed estuary*. Journal of Physical Oceanography, 30(8), 2035-2048. doi:Doi 10.1175/1520-0485(2000)030<2035:Tdoapm>2.0.Co;2
Gong, W. P., Maa, J. P. Y., Hong, B., & Shen, J. (2014). Salt transport during a dry season in the modaomen estuary, pearl river delta, china. Ocean & Coastal Management, 100, 139-150. doi:10.1016/j.ocecoaman.2014.03.024
Gong, W. P., & Shen, J. (2011). The response of salt intrusion to changes in river discharge and tidal mixing during the dry season in the modaomen estuary, china. Continental Shelf Research, 31(7-8), 769-788. doi:10.1016/j.csr.2011.01.011
Hansen, D. V., & Rattray, M. (1965). Gravitational circulation in straits and estuaries.
Hansen, D. V., & Rattray, M. (1966). New dimensions in estuary classification. Limnology and oceanography, 11(3), 319-326.
He, W., Zhang, J., Yu, X., Chen, S., & Luo, J. J. W. R. R. (2018). Effect of runoff variability and sea level on saltwater intrusion: A case study of nandu river estuary, china. 54(12), 9919-9934.
Hetland, R. D., & Geyer, W. R. (2004). An idealized study of the structure of long, partially mixed estuaries*. Journal of Physical Oceanography, 34(12), 2677-2691.
Hunkins, K. (1981). Salt dispersion in the hudson estuary. Journal of Physical Oceanography, 11(5), 729-738. doi:10.1175/1520-0485(1981)011<0729:SDITHE>2.0.CO;2
Jassby, A. D., Kimmerer, W. J., Monismith, S. G., Armor, C., Cloern, J. E., Powell, T. M., . . . Vendlinski, T. J. J. E. a. (1995). Isohaline position as a habitat indicator for estuarine populations. 5(1), 272-289.
Jay, D. A., & Smith, J. D. (1990). Circulation, density distribution and neap-spring transitions in the columbia river estuary. Progress in Oceanography, 25(1-4), 81-112. doi:10.1016/0079-6611(90)90004-l
Kennish, M. (1986). Estuarine ecology. In: Boca Raton, Florida,

United States: CRC Press.
Ketchum, B. 1983: Estuaries and enclosed seas. In: Elsevier Scientific, Amsterdam.
Kim, B. G., & Cho, Y. K. (2017). Tide-induced residual circulation in a bay with laterally asymmetric depth. Journal of Geophysical Research: Oceans, 122(5), 4040-4050.
Large, W. G., McWilliams, J. C., & Doney, S. C. (1994). Oceanic vertical mixing: A review and a model with a nonlocal boundary layer parameterization. Reviews of Geophysics, 32(4), 363-403. doi:10.1029/94RG01872
Lee, M., Park, B. S., Baek, S. H. J. E., & Coasts. (2018). Tidal influences on biotic and abiotic factors in the seomjin river estuary and gwangyang bay, korea. 41(7), 1977-1993.
Lerczak, J. A., Geyer, W. R., & Chant, R. J. (2006). Mechanisms driving the time-dependent salt flux in a partially stratified estuary. Journal of Physical Oceanography, 36(12), 2296-2311. doi:10.1175/jpo2959.1
Lerczak, J. A., Geyer, W. R., & Ralston, D. K. (2009). The temporal response of the length of a partially stratified estuary to changes in river flow and tidal amplitude. Journal of Physical Oceanography, 39(4), 915-933. doi:10.1175/2008jpo3933.1
Lewis, R. E., & Uncles, R. J. (2003). Factors affecting longitudinal dispersion in estuaries of different scale. Ocean Dynamics, 53(3), 197-207. doi:10.1007/s10236-003-0030-2
Li, C., & O'Donnell, J. (2005). The effect of channel length on the residual circulation in tidally dominated channels. Journal of Physical Oceanography, 35(10), 1826-1840. doi:10.1175/JPO2804.1
Li, C. Y., & O'Donnell, J. (1997). Tidally driven residual circulation in shallow estuaries with lateral depth variation. Journal of Geophysical Research-Oceans, 102(C13), 27915-27929. doi:10.1029/97jc02330
Li, M., & Zhong, L. J. (2009). Flood-ebb and spring-neap variations of mixing, stratification and circulation in chesapeake bay. Continental Shelf Research, 29(1), 4-14. doi:10.1016/j.csr.2007.06.012
Li, X., Geyer, W. R., Zhu, J., & Wu, H. (2018). The transformation of salinity variance: A new approach to quantifying the influence of straining and mixing on estuarine stratification. Journal of Physical Oceanography, 48(3), 607-623. doi:10.1175/JPO-D-17-0189.1

Linden, P., & Simpson, J. (1988). Modulated mixing and frontogenesis in shallow seas and estuaries. Continental Shelf Research, 8(10), 1107–1127.

Liu, W.–C., Chen, W.–B., Cheng, R. T., Hsu, M.–H., & Kuo, A. Y. J. C. S. R. (2007). Modeling the influence of river discharge on salt intrusion and residual circulation in danshuei river estuary, taiwan. 27(7), 900–921. doi:10.1016/j.csr.2006.12.005

MacCready, P. (2007). Estuarine adjustment. Journal of Physical Oceanography, 37(8), 2133–2145. doi:10.1175/jpo3082.1

MacCready, P. (2011). Calculating estuarine exchange flow using isohaline coordinates. Journal of Physical Oceanography, 41(6), 1116–1124. doi:10.1175/2011jpo4517.1

MacCready, P., & Geyer, W. R. (2010). Advances in estuarine physics. Annual Review of Marine Science, 2, 35–58. doi:10.1146/annurev–marine–120308–081015

Mantovanelli, A., Marone, E., da Silva, E. T., Lautert, L. F., Klingenfuss, M. S., Prata, V. P., . . . Angulo, R. J. (2004). Combined tidal velocity and duration asymmetries as a determinant of water transport and residual flow in paranagua bay estuary. Estuarine Coastal and Shelf Science, 59(4), 523–537. doi:10.1016/j.ecss.2003.09.001

Masson, D., & Cummins, P. F. (2000). Fortnightly modulation of the estuarine circulation in juan de fuca strait. Journal of Marine Research, 58(3), 439–463. doi:Doi 10.1357/002224000321511106

Monismith, S., Burau, J., & Stacey, M. (1996). Stratification dynamics and gravitational circulation in northern san francisco bay. San Francisco Bay: The Ecosystem, 123–153.

Monismith, S. G., Kimmerer, W., Burau, J. R., & Stacey, M. T. J. J. o. P. O. (2002). Structure and flow–induced variability of the subtidal salinity field in northern san francisco bay. 32(11), 3003–3019.

Officer, C. (1976). Physical oceanography of estuaries john wiley & sons. New York, 4, 65.

P MacCready and NS Banas. (2011). Residual circulation, mixing, and dispersion.

Park, K., & Kuo, A. Y. (1996). Effect of variation in vertical mixing on residual circulation in narrow, weakly nonlinear estuaries. Buoyancy effects on coastal and estuarine dynamics, 301–317.

Pein, J. U., Stanev, E. V., & Zhang, Y. J. (2014). The tidal asymmetries and residual flows in ems estuary. Ocean

Dynamics, 64(12), 1719-1741. doi:10.1007/s10236-014-0772-z
Prandle, D. (1985). On salinity regimes and the vertical structure of residual flows in narrow tidal estuaries. Estuarine, Coastal and Shelf Science, 20(5), 615-635.
Prandle, D. (2004). Saline intrusion in partially mixed estuaries. Estuarine, Coastal and Shelf Science, 59(3), 385-397. doi:10.1016/j.ecss.2003.10.001
Pritchard, D. W. (1952). Salinity distribution and circulation in the chesapeake bay estuarine system. Journal of Marine Research, 11(2), 106-123.
Pritchard, D. W. (1967). What is an estuary: Physical viewpoint.
Pu, X., Shi, J. Z., Hu, G.-D., & Xiong, L.-B. (2015). Circulation and mixing along the north passage in the changjiang river estuary, china. Journal of Marine Systems, 148, 213-235. doi:10.1016/j.jmarsys.2015.03.009
Ralston, D. K., Geyer, W. R., & Lerczak, J. A. (2008). Subtidal salinity and velocity in the hudson river estuary: Observations and modeling. Journal of Physical Oceanography, 38(4), 753-770. doi:10.1175/2007jpo3808.1
Ralston, D. K., Geyer, W. R., & Lerczak, J. A. (2010). Structure, variability, and salt flux in a strongly forced salt wedge estuary. Journal of Geophysical Research-Oceans, 115. doi:10.1029/2009jc005806
Ralston, D. K., & Stacey, M. T. (2005). Longitudinal dispersion and lateral circulation in the intertidal zone. Journal of Geophysical Research-Oceans, 110(C7). doi:10.1029/2005jc002888
Rayson, M. D., Gross, E. S., Hetland, R. D., & Fringer, O. B. (2017). Using an isohaline flux analysis to predict the salt content in an unsteady estuary. Journal of Physical Oceanography, 47(11), 2811-2828. doi:10.1175/jpo-d-16-0134.1
Ross, L., Valle-Levinson, A., Sottolichio, A., & Huybrechts, N. (2017). Lateral variability of subtidal flow at the mid-reaches of a macrotidal estuary. Journal of Geophysical Research-Oceans, 122(9), 7651-7673. doi:10.1002/2016jc012504
Schettini, C. A. F., Ricklefs, K., Truccolo, E. C., & Golbig, V. (2006). Synoptic hydrography of a highly stratified estuary. Ocean Dynamics, 56(3-4), 308-319. doi:10.1007/s10236-006-0066-1
Schulz, E., Schuttelaars, H. M., Gräwe, U., & Burchard, H. (2015). Impact of the depth-to-width ratio of periodically stratified

tidal channels on the estuarine circulation. Journal of Physical Oceanography, 45(8), 2048-2069. doi:10.1175/jpo-d-14-0084.1

Scully, M. E., Friedrichs, C., & Brubaker, J. (2005). Control of estuarine stratification and mixing by wind-induced straining of the estuarine density field. Estuaries, 28(3), 321-326. doi:10.1007/bf02693915

Scully, M. E., Geyer, W. R., & Lerczak, J. A. (2009). The influence of lateral advection on the residual estuarine circulation: A numerical modeling study of the hudson river estuary. Journal of Physical Oceanography, 39(1), 107-124. doi:10.1175/2008jpo3952.1

Shaha, D., & Cho, Y.-K. (2009). Comparison of empirical models with intensively observed data for prediction of salt intrusion in the sumjin river estuary, korea. Hydrology and Earth System Sciences, 13(6), 923-933. doi:DOI 10.5194/hess-13-923-2009

Shaha, D. C., Cho, Y. K., & Kim, T. W. (2013). Effects of river discharge and tide driven sea level variation on saltwater intrusion in sumjin river estuary: An application of finite-volume coastal ocean model. Journal of Coastal Research, 29(2), 460-470. doi:10.2112/jcoastres-d-12-00135.1

Shchepetkin, A. F., & McWilliams, J. C. (2005). The regional oceanic modeling system (roms): A split-explicit, free-surface, topography-following-coordinate oceanic model. Ocean Modelling, 9(4), 347-404. doi:10.1016/j.ocemod.2004.08.002

Simpson, J. H., Brown, J., Matthews, J., & Allen, G. (1990). Tidal straining, density currents, and stirring in the control of estuarine stratification. Estuaries, 13(2), 125-132. doi:Doi 10.2307/1351581

Stacey, M. T., Brennan, M. L., Burau, J. R., & Monismith, S. G. (2010). The tidally averaged momentum balance in a partially and periodically stratified estuary. Journal of Physical Oceanography, 40(11), 2418-2434. doi:10.1175/2010jpo4389.1

Stacey, M. T., Burau, J. R., & Monismith, S. G. (2001). Creation of residual flows in a partially stratified estuary. Journal of Geophysical Research, 106(C8), 17013. doi:10.1029/2000jc000576

Stanev, E. V., Al-Nadhairi, R., & Valle-Levinson, A. (2015). The

role of density gradients on tidal asymmetries in the german bight. Ocean Dynamics, 65(1), 77-92. doi:10.1007/s10236-014-0784-8

Talke, S. A., de Swart, H. E., & Schuttelaars, H. M. (2009). Feedback between residual circulations and sediment distribution in highly turbid estuaries: An analytical model. Continental Shelf Research, 29(1), 119-135. doi:10.1016/j.csr.2007.09.002

Toublanc, F., Brenon, I., Coulombier, T., & Le Moine, O. (2015). Fortnightly tidal asymmetry inversions and perspectives on sediment dynamics in a macrotidal estuary (charente, france). Continental Shelf Research, 94, 42-54. doi:10.1016/j.csr.2014.12.009

Turrell, W., Brown, J., & Simpson, J. (1996). Salt intrusion and secondary flow in a shallow, well-mixed estuary. Estuarine, Coastal and Shelf Science, 42(2), 153-169.

Uncles, R., & Stephens, J. (1996). Salt intrusion in the tweed estuary. Estuarine, Coastal and Shelf Science, 43(3), 271-293.

Uncles, R. J., & Stephens, J. A. (1990). The structure of vertical current profiles in a macrotidal, partly-mixed estuary. Estuaries, 13(4), 349-361. doi:10.2307/1351780

Valle-Levinson, A. (2010). Contemporary issues in estuarine physics: Cambridge University Press.

Valle-Levinson, A. (2011). Classification of estuarine circulation.

Valle-Levinson, A., & Schettini, C. A. (2016). Fortnightly switching of residual flow drivers in a tropical semiarid estuary. Estuarine, Coastal and Shelf Science, 169, 46-55.

Vaz, N., Leitao, P. C., & Dias, J. M. (2007). Channel-ocean exchange driven by tides and river flow: Espinheiro channel (portugal). Journal of Coastal Research, 1000-1004.

Wang, A. H.-J., Quigley, G. J., Kolpak, F. J., Crawford, J. L., Van Boom, J. H., van der Marel, G., & Rich, A. J. N. (1979). Molecular structure of a left-handed double helical DNA fragment at atomic resolution. 282(5740), 680.

Wang, D.-P., & Elliott, A. (1978). Non-tidal variability in the chesapeake bay and potomac river: Evidence for non-local forcing. Journal of Physical Oceanography, 8(2), 225-232.

Warner, J. C., Geyer, W. R., & Lerczak, J. A. (2005). Numerical modeling of an estuary: A comprehensive skill assessment. Journal of Geophysical Research-Oceans, 110(C5). doi:10.1029/2004jc002691

Wei, X., Schuttelaars, H. M., Williams, M. E., Brown, J. M., Thorne, P.

D., & Amoudry, L. O. (2021). Unraveling interactions between asymmetric tidal turbulence, residual circulation, and salinity dynamics in short, periodically weakly stratified estuaries. Journal of Physical Oceanography, 51(5), 1395-1416. doi:10.1175/JPO-D-20-0146.1

Weisberg, R. H., & Zheng, L. (2003). How estuaries work: A charlotte harbor example. Journal of Marine Research, 61(5), 635-657. doi:Doi 10.1357/002224003771815981

Willmott, C. J. (1981). On the validation of models. Physical geography, 2(2), 184-194.

Wong, K.-C., & Valle-Levinson, A. (2002). On the relative importance of the remote and local wind effects on the subtidal exchange at the entrance to the chesapeake bay. Journal of Marine Research, 60(3), 477-498.

Xue, P. F., Chen, C. S., Ding, P. X., Beardsley, R. C., Lin, H. C., Ge, J. Z., & Kong, Y. Z. (2009). Saltwater intrusion into the changjiang river: A model-guided mechanism study. Journal of Geophysical Research-Oceans, 114. doi:10.1029/2008jc004831

Zhong, L., & Li, M. (2006). Tidal energy fluxes and dissipation in the chesapeake bay. Continental Shelf Research, 26(6), 752-770. doi:10.1016/j.csr.2006.02.006

Abstract (in Korean)

하구에서 교환류는 주로 수평염분구배와 조석에 의한 수직혼합의 경합 결과로 결정되며, 하구의 소금, 영양분, 오염 물질 및 부유 퇴적물의 분포에 주요한 역할을 한다. 교환류의 수직 전단의 강도는 수평염분구배에 따라 결정된다. 본 논문에서는 섬진강 하구에서 강제력의 다양한 조건에서 관측자료와 수치모델을 사용하여 교환류와 수평염분구배의 시공간 변화를 분석하고 그 변화 매커니즘에 대해 연구하였다.

많은 하구들과 달리, 섬진강 하구의 하부에서 관측한 교환류의 수직전단은 소조보다 대조에 더 강했다. 해석 모델을 사용하여 교환류의 결정 요인을 분석해본 결과, 대조 동안에 염분구배의 강화로 인한 효과가 수직적으로 균일하게 만드는 수직혼합 효과보다 컸다.

하구의 다른 위치에서도 교환류의 대소조 변화와 그 결정요인에 대해 알아보기 위해, 3차원 수치 모델(ROMS)을 사용하여 지형 변화를 단순화 해서 하구 전체를 구현하였다. 수치모델 결과는 관측한 염분과 유속 결과와 비교하여 검증하였다. 염분구배와 교환류는 대소조 조석 주기 동안 하구의 상부와 하부 사이에서 서로 다른 시간 변화를 했다. 수직혼합에 의해 결정되는 염분의 플럭스의 변화 결과로 인해 최대 염분구배는 하구의 채널을 따라 주기적으로 왕복 이동을 한다. 최대 염분구배가 하구의 상부와 하부에서의 위상이 다르기 때문에 교환류의

위상도 하구의 위치에 따라 다르다. 조차가 감소하는 동안에, 수직 혼합 효과를 압도할만큼 큰 염분구배가 하구의 입구에서부터 하구안쪽으로 이동함에 따라 교환류가 강한 곳도 유사한 위치 변화를 한다. 강한 교환류의 시공간 변화와 비교적 잘 일치하는 높은 수평 리차드슨 수는 교환류의 시공간 변화는 염분구배에 의해 결정됨을 증명했다.

위 결과들은 유량이 고정되어 있다는 한계가 있고 실제 하구는 다양한 유량 상황에 놓여 있으므로, 유량이 낮을때부터 높을동안 교환류의 변화와 주요 원인을 알아보았다. 교환류을 결정하는 주요인이였던 수평염분구배는 유량과 조차에 따라 달라지는 염분포에 의해 결정되었다. 유량이 낮을때부터 높을때까지 염분포의 대소조 변화를 분석하였다. 유량이 낮을때에는 염분포의 대소조 변화가 뚜렷하지 않지만, 유량이 증가함에 따라 대소조에 따른 변화는 뚜렷하며, 염이 유출되다가 유입으로 전환되는 시기가 대조에 가까워졌다. 증가한 유량은 하구 밖으로의 염 유출을 늘려서 염 유입 거리가 짧아지게 한다. 하지만 이로 인해 대조에 하구의 하부에서 염분구배가 커짐에 따라 경압력에 의한 교환류의 강화로 염 수송이 바다쪽에서 육지쪽으로 전환되는데, 이 시기가 유량이 늘어남에 따라 빨라지게 된 것이다. 교환류의 대소조 변화를 결정하는 주 요인은 유량에 따라 달라졌다. 유량이 낮을때는 수직혼합 이지만, 평균 이상의 유량에서는 염분구배가 주요인이었다.